



**This is a self-archived version of an original article. This version may differ from the original in pagination and typographic details.**

**Author(s):** Vernon, A. R.; Billowes, J.; Binersley, C. L.; Bissell, M. L.; Cocolios, T. E.; Farooq-Smith, G. J.; Flanagan, K. T.; Ruiz, R. F. Garcia; Gins, W.; de Groote, Ruben; Koszorús, Á.; Lynch, K. M.; Neyens, G.; Ricketts, C. M.; Wendt, K. D. A.; Wilkins, S. G.; Yang, X. F.

**Title:** Simulation of the relative atomic populations of elements  $1 \leq Z \leq 89$  following charge exchange tested with collinear resonance ionization spectroscopy of indium

**Year:** 2019

**Version:** Published version

**Copyright:** © 2019 The Authors

**Rights:** CC BY 4.0

**Rights url:** <https://creativecommons.org/licenses/by/4.0/>

**Please cite the original version:**

Vernon, A. R., Billowes, J., Binersley, C. L., Bissell, M. L., Cocolios, T. E., Farooq-Smith, G. J., Flanagan, K. T., Ruiz, R. F. G., Gins, W., de Groote, R., Koszorús, Á., Lynch, K. M., Neyens, G., Ricketts, C. M., Wendt, K. D. A., Wilkins, S. G., & Yang, X. F. (2019). Simulation of the relative atomic populations of elements  $1 \leq Z \leq 89$  following charge exchange tested with collinear resonance ionization spectroscopy of indium. *Spectrochimica Acta Part B: Atomic Spectroscopy*, 153, 61-83. <https://doi.org/10.1016/j.sab.2019.02.001>



# Simulation of the relative atomic populations of elements $1 \leq Z \leq 89$ following charge exchange tested with collinear resonance ionization spectroscopy of indium



A.R. Vernon<sup>a,\*</sup>, J. Billowes<sup>a</sup>, C.L. Binersley<sup>a</sup>, M.L. Bissell<sup>a</sup>, T.E. Cocolios<sup>d</sup>, G.J. Farooq-Smith<sup>d</sup>, K.T. Flanagan<sup>a,c</sup>, R.F. Garcia Ruiz<sup>a,b</sup>, W. Gins<sup>d</sup>, R.P. de Groot<sup>g,d</sup>, Á. Koszorús<sup>d</sup>, K.M. Lynch<sup>b</sup>, G. Neyens<sup>d</sup>, C.M. Ricketts<sup>a</sup>, K.D.A. Wendt<sup>e</sup>, S.G. Wilkins<sup>a</sup>, X.F. Yang<sup>d,f</sup>

<sup>a</sup> School of Physics and Astronomy, The University of Manchester, Manchester M13 9PL, United Kingdom

<sup>b</sup> ISOLDE, EP Department, CERN, CH-1211, Geneva-23, Switzerland

<sup>c</sup> Photon Science Institute Alan Turing Building, University of Manchester, Manchester M13 9PY, United Kingdom

<sup>d</sup> KU Leuven, Instituut voor Kern- en Stralingsfysica, B-3001 Leuven, Belgium

<sup>e</sup> Institut für Physik, Johannes Gutenberg-Universität Mainz, D-55128 Mainz, Germany

<sup>f</sup> School of Physics, State Key Laboratory of Nuclear Physics and Technology, Peking University, Beijing 100871, China

<sup>g</sup> Department of Physics, University of Jyväskylä, Survontie 9, Jyväskylä FI-40014, Finland

## ARTICLE INFO

### Keywords:

Laser spectroscopy  
Collinear resonance ionization spectroscopy  
Indium  
Sodium  
Potassium  
Electron capture  
Atomic populations  
Charge exchange  
Semi-classical impact parameter

## ABSTRACT

Calculations of the neutralisation cross-section and relative population of atomic states were performed for ions beams ( $1 \leq Z \leq 89$ ) at 5 and 40 keV incident on free sodium and potassium atoms. To test the validity of the calculations, the population distribution of indium ions incident on a vapour of sodium was measured at an intermediate energy of 20 keV. The relative populations of the  $5s^25p\ ^2P_{1/2}$  and  $5s^25p\ ^2P_{3/2}$  states in indium were measured using collinear resonance ionization spectroscopy and found to be consistent with the calculations. Charge exchange contributions to high-resolution lineshapes were also investigated and found to be reproduced by the calculations. The reliable prediction of relative populations and reproduction of lineshapes are of importance to high-precision and efficient laser spectroscopy studies of exotic isotopes and future applications of collinear resonance ionization spectroscopy.

## 1. Introduction

Many collinear laser spectroscopy (CLS) measurements are performed on atomic rather than ionic beams, in part due to the availability of spectroscopic data but also, in the case of collinear resonance ionization spectroscopy [1,2] (CRIS), due to the lower ionization potential (IP) of atomic systems. This reduces the technical complexity of step-wise laser-ionization as well the ion optics required. Producing a neutral atom beam is typically done through electron-capture reactions with an alkali vapour. During these reactions several atomic states may be populated.

Reliable simulation of the population distribution is of crucial importance in predicting the total measurement efficiency of an experiment for a given ionic ensemble. This is particularly important for CLS measurements at radioactive ion beam facilities such as CERN-ISOLDE [3] where all experimental losses have to be well understood in order to

perform measurements on nuclei with low production yields [4]. Nevertheless, comprehensive experimental data and theoretical predictions of relative populations in this energy regime are largely unavailable, or not reported on. The simulation and measurement of this distribution for ion beam energies in the order 1–100 keV is the subject of this paper.

Calculation of the electron-capture cross sections were performed using the semi classical approach by Rapp and Francis [5] (R&F). This provided the initial populations following charge exchange which were then used to predict final populations following spontaneous decay. These calculations were performed for neutralisation of all elements from hydrogen to thorium. However, the R&F approach uses simplified hydrogen-like orbitals [6,7] among other approximations detailed in Section 2. Benchmarking these calculations with measurements is crucial for gaining confidence in extending them to these multi-electron systems.

\* Corresponding author.

E-mail addresses: adam.vernon@cern.ch, adam.vernon-2@postgrad.manchester.ac.uk (A.R. Vernon).

When choosing an alkali metal for neutralisation it is common practice to match the IP of the element to be neutralised with the alkali metal. While this ensures a large relative population in the ground state of the product atom, it does not guarantee the highest total cross section for neutralisation nor does it guarantee the highest relative population of the ground state. This is because it does not take into account the density of states near the IP difference of the product atom and alkali metal, the electronic angular momentum of the states or their lifetime. Measurement of the relative populations of atomic indium following neutralisation with a sodium vapour at 20 keV was used as an exemplar case in this work. The maximum beam energy was limited experimentally, however the measurements at 20 keV act as an intermediate benchmark for the simulations at 5 keV and 40 keV.

The accessibility of two low lying states by neighbouring wavelength atomic transitions (246.0 nm and 246.8 nm) and a difference in IP of 0.6 eV from sodium makes these states in indium a good test of both cross section calculations and simulated feeding from higher lying states following charge exchange.

Furthermore, as indium is solid at room temperature this allowed for the use of an ablation-ion-source setup [1], which also highlights the applicability of this work to spectrochemical analysis of solid samples, especially in trace analysis where the sensitivity and selectivity of the CRIS technique could excel [1,8].

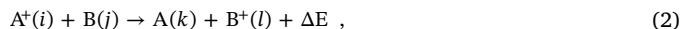
## 2. Atomic charge exchange

This section will introduce the key concepts of the atomic charge-exchange reactions used to neutralise ion beams. Neutralisation of an ion beam  $A^+$  takes place when an electron is captured from a free atom B. Often B is chosen as a low-IP element e.g. sodium or potassium. In principle the gaseous form of any element can be used. Molecules such as isobutane are also routinely used at accelerator mass spectrometry facilities [9] as they enhance negative ion production.

In resonant symmetric charge exchange  $B^+ + B \rightarrow B + B^+$  reactions, where the ion and atom are the same element, the cross section for electron capture is the highest, and decreases with the beam energy  $T_B$  (keV) as

$$\sigma_{CE}^{1/2} = a - b \ln T_B . \quad (1)$$

In this expression  $a$  and  $b$  are constants, which are typically empirically fitted to available charge-exchange cross sections for an element [7,10–12]. In the symmetric case the highest cross section will be for the reaction that neutralizes the ion into its atomic ground state. However for many purposes electron capture of the ion will be from a dissimilar element, proceeding by an asymmetric charge-exchange reaction



where  $A^+(i)$  is the ion in an electronic state  $i$ , which picks up an electron from a free atom  $B(j)$  in its electronic state  $j$ , leaving A in an excited state  $k$  after the reaction and B in an excited state  $l$ . For these simulations it is assumed that  $A^+$ , B and  $B^+$  are all in their electronic ground states. These electronic states  $k$  can be significantly higher in energy than the ground state depending on the difference in IP of the reactant ion and atom  $\Delta E = I_A - I_B$ . For the beam energies of interest for CLS ( $> 5$  keV) this energy deficit does not significantly reduce the cross section for charge exchange, and thus many of these high lying states can be populated in asymmetric charge exchange.

The maximum cross section  $\sigma_{CE}$  for an asymmetric charge-exchange reaction with energy deficit  $\Delta E$  can approximately be found at a velocity

$$v \approx \frac{a\Delta E}{h} , \quad (3)$$

from Massey's hypothesis [13], where  $h$  is the Planck constant. This hypothesis assumes an *adiabatic* region of velocities where the

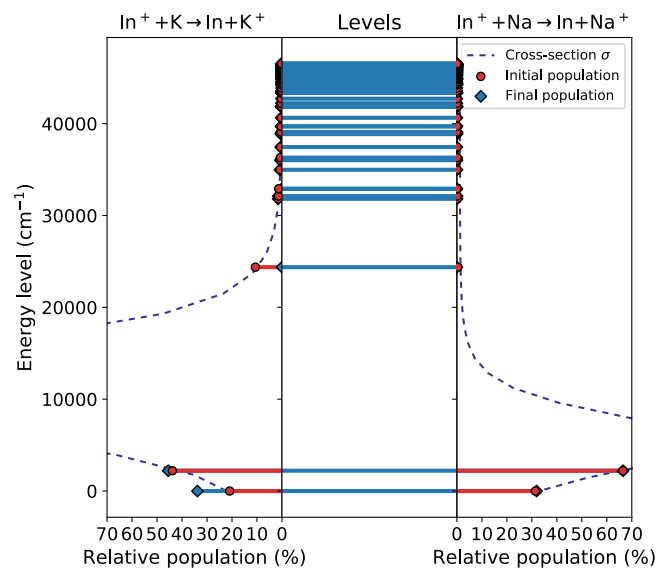


**Fig. 1.** Initial and final electronic state populations of In I compared for neutralisation by Na I or K I. For a beam energy  $T_B = 20$  keV and with de-excitation following an atom flight length of  $l_{\text{flight}} = 120$  cm. The  $^2P_{3/2}$  and  $^2P_{1/2}$  states have cross sections of  $\sigma(^2P_{3/2}) = 4.17 \times 10^{-15} \text{ cm}^2$  and  $\sigma(^2P_{1/2}) = 1.97 \times 10^{-15} \text{ cm}^2$  using sodium or  $\sigma(^2P_{3/2}) = 3.93 \times 10^{-16} \text{ cm}^2$  and  $\sigma(^2P_{1/2}) = 1.88 \times 10^{-16} \text{ cm}^2$  using potassium.

characteristic electronic-transition time is much shorter than the collision of the reactants from their relative velocity, allowing for readjustment of the electronic motion, without transition as the internucleon distance reduces. At the velocity of Eq. (3) this is no longer the case and  $\sigma_{CE}$  becomes maximum, before decreasing with increasing incident beam energy. An adiabatic parameter of  $a = 7 \times 10^{-8} \text{ cm}$  has been found to be consistent with many reactions [12,14–16].

It is the relative cross section for these reactions into individual atomic states that is of interest for CLS experiments as they determine the population distribution of states from which measurements can be performed. This process is represented in Fig. 1 for indium where the initial population distribution has evolved after 120 cm of atom flight, from 6.55  $\mu\text{s}$  of spontaneous decay, as detailed in Section 2.2. Another interesting application requiring knowledge of neutralisation cross-sections, which can easily be seen with Eq. (3), is for ultrasensitive detection techniques of radioisotopes. By tuning the velocity of the ion beam and by optical pumping of the electronic populations of the ion or atom, the cross section can be manipulated for state-selective neutralisation [17,18].

The efficiency for neutralisation of an ion beam can be estimated with a simple attenuation model [15] as

$$\epsilon_{CE} = 1 - \exp(-n\sigma_{CE}L) \quad (4)$$

where  $n$  is the alkali atom number density and  $L$  is the effective interaction path length. They depend on the geometry of the vapour cell [19–21] and can be estimated with empirical vapour pressure relations [22] with temperature measurements. The total cross section for neutralisation  $\sigma_{CE}$  depends on the initial atomic systems  $A^+(i)$ ,  $B(j)$  and can proceed through multiple channels.

A method to calculate the cross section for asymmetric charge-exchange reactions using a semi-classical impact-parameter approach was developed by R&F [5]. This method is used to calculate neutralisation cross-sections in this paper and is detailed in Section 2.1. In the impact parameter treatment [23,24] the linear trajectory of projectile is assumed to not be altered by electron pick up. Although this is a good approximation for calculation as the de Broglie wavelength of the incident ion is small, in practice significant deflections of the product atom have been observed. For example with  $O^+ + N_2$  [25] where the

energy deficit for the reaction to the ground state to proceed is large, closer collisions are required, which results in larger scattering angles of up to 3°.

In a three-body approximation of the electron in the field of the target and projectile atoms, the Schrödinger equation determines the evolution of the three-body collisional system as a function of time,  $t$  for fixed values of impact parameter  $b$  and incident velocity  $v$ . Thus, the probability for electron capture can be formulated in terms of parameters  $b$  and  $t$ .

This approximate approach does not include many contributions of more recent and complete theories [26,27,28]. For instance, inclusion of the long-range Coulomb interaction was found to be important for convergence of perturbation expansions [29]. Furthermore, of the possible channels for electron capture, the impact-parameter approach only considers the non-radiative kinematic mechanism of [30,23]. Radiative channels in which the electron is captured due to the emission of a photon [31] or in which electron capture is accompanied by the emission of another electron [32] have also been identified as first-order electron-transfer mechanisms. For symmetric charge-exchange reaction cross sections, a large amount of experimental data has been compiled in [33]. For atoms with IPs much lower than hydrogen and beam energies of < 5 keV/u, where R&F calculations show poor agreement, a simple relationship was found [34] that proved to be a successful correction to the calculations [35,36]. Another correction, to the one-electron potential, determined using a linear combination of hydrogenic orbitals [37] has been noticed and applied by [38] and found to be in good agreement for both single- and double-electron symmetric charge exchange [38,39]. It is worth noting that cross-section calculations including the four-body interactions explicitly for cases of both single- and double-electron capture are now also possible [40,41,42].

Although the absolute agreement of the cross sections with experiment using the R&F method is known to be poor in some cases, the method has proved useful in reproducing the ion velocity dependence of the cross sections in asymmetric charge-exchange [43,35,39,44]. This is particularly important for calculation of relative populations, where relative cross sections for thousands of atomic states needs to be calculated, for some elements, to predict the initial populations. In these calculations, the largest uncertainty will be due to missing spectroscopic data. The R&F method has already successfully been applied to this end [45,19].

### 2.1. Cross-section calculations

The R&F method formulates the cross section for electron capture between species with an IP difference of  $\Delta E = I_A - I_B = \omega\hbar$  to be dependent on incident velocity  $v$  and impact parameter  $b$  as

$$\sigma(b, v) = 2\pi \int_0^\infty P_\omega(b, v) b db \quad (5)$$

with the asymmetric charge-exchange probability  $P_\omega(b, v)$  given by

$$P_\omega(b, v) = f P_0(b, v) \operatorname{sech}\left(\frac{\omega}{v} \sqrt{\frac{a_0 \pi b}{2\gamma}}\right)^2 \quad (6)$$

where  $f = f_{SL}$  is a statistical weighting factor to take into account the ratio of multiplicity between the products spin and orbital angular momenta and that possible for forming the reactants. The symmetric charge-exchange probability  $P_0(b, v)$  is defined as

$$P_0(b, v) = \sin\left(\sqrt{\frac{2\pi}{\gamma a_0} \frac{2\bar{I}}{b^2}} \left(1 + \frac{a_0}{\gamma b}\right) \exp\left(\frac{-\gamma b}{a_0}\right)\right)^2 \quad (7)$$

where  $\bar{I} = \frac{I_A + I_B}{2}$  is the average atom IP of the reactant elements,  $\gamma = \sqrt{\frac{T}{13.6}}$  and  $a_0$  is the Bohr radius. A factor of 2 correction is included inside the sine compared to the original formulation [5], this was found to be necessary by [46].

These formulations [5] were made under the assumption of an ‘intermediate’ beam energy ( $T_B$ ) region [47] taken to be

$$m_B \text{ meV} < T_B < 10 m_B \text{ keV} \quad (8)$$

where  $m_B$  is the mass of the incident ion in atomic mass units. While hydrogen and helium are on the boundary for this assumption, all other possible incident element masses at beam energies typical for CLS experiments are well covered by this region.

Using the R&F method the cross section for neutralisation from the ground state in the reactant ion and atom electronic states to all known neutralised atom product states was calculated for indium in addition to all other elements from hydrogen to actinium ( $Z = 89$ ). The atomic structure information was taken from the NIST atomic database [48]. For elements where very little transition information was available, only the initial population distribution prior to decay is reported. The numerical integration was performed with the help of a Levin-type [49] approximation for highly oscillatory integrals, which removed the need for the approximation of  $P_0(b, v) = \frac{1}{2}$  and the need for solving separately for its cut-off impact parameter [5] for each electronic state. This step allowed automation of the calculations.<sup>1</sup>

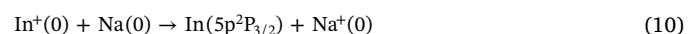
### 2.2. Relative atomic populations

After the charge-exchange cross section  $\sigma_{CE}$  is calculated for each state, the subsequent de-excitation to lower levels over a distance  $l_{\text{flight}}$  between the charge exchange cell and interaction region for a beam velocity  $v$  is calculated. The Einstein spontaneous decay coefficients  $A_{ki}$  needed to simulate the decay schemes were taken from the NIST atomic database [48]. The biggest source of error in these calculations is from neglected levels or  $A_{ki}$  coefficient information. Transitions with unknown  $A_{ki}$  coefficients were not used in the simulation. This source of systematic error is difficult to evaluate, but the unknown de-excitation paths will result in an overestimation of the population of higher-lying states which would have been transferred to lower-lying states in reality. The  $A_{ki}$  coefficients were used to calculate the branching ratios  $\beta_{ki'} = \frac{A_{ki'}}{\sum_i A_{ki'}}$  to each lower state  $i$  and the population was then evolved using the simple relation for fractional change for each upper state  $k$

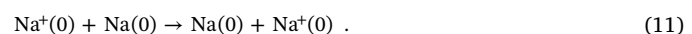
$$F_k^{\text{decay}} = \exp\left(-\frac{l_{\text{flight}}}{v} \sum_i A_{ki}\right) \quad (9)$$

which allowed the intermediate state information to be tracked with each step of the spontaneous-decay simulation.

It is instructive to compare the cross section for the population of a state and its relative atomic population as a function of ion beam energy for an example asymmetric reaction with a large difference in the element IPs



as well as for an example symmetric reaction



The results are shown in Fig. 2. In the latter case the cross-section for the direct population of the product sodium ground state as well as the relative population simply increases with decreasing beam energy, as one would expect from Eq. (3) and which is experimentally well established [33,5]. As the reaction moves away from resonant conditions at  $T_B = 0$  keV the contribution to the final population enabled by population of nearby states increases significantly, despite a reduction

<sup>1</sup> The authors code used to perform the calculations in this work, as well as a larger compilation of results, can be found at <https://github.com/adamrobertvernon/chargeexchange> and can be freely used, provided this work is referenced. Only the five most populated states are shown in the Tables 2 and 3 at the end of this paper, the remaining populations can be found online

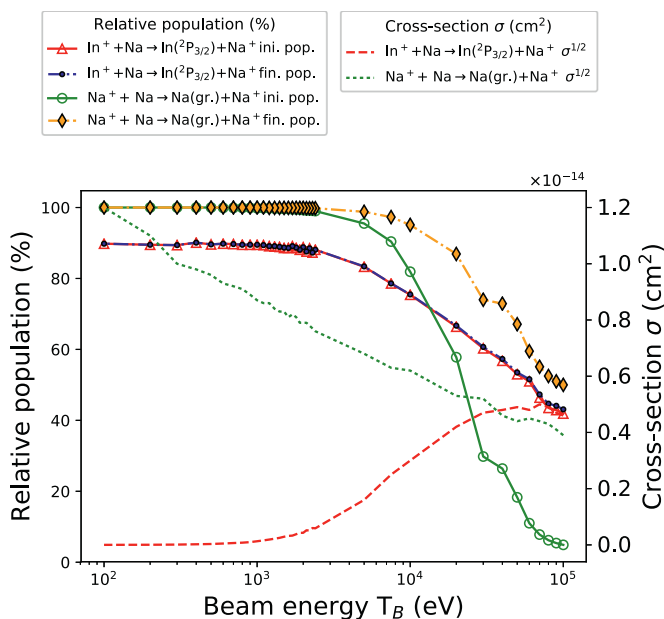


**Fig. 2.** Initial and final electronic state populations and cross-sections for the reactions  $\text{In}^+ + \text{Na} \rightarrow \text{In}(5\text{p}^2\text{P}_{3/2}) + \text{Na}^+$  and  $\text{Na}^+ + \text{Na} \rightarrow \text{Na}(\text{ground}) + \text{Na}^+$ . For beam energies in the range  $T_B = 0\text{--}100 \text{ keV}$  and with de-excitation following an atom flight length of  $l_{\text{flight}} = 120 \text{ cm}$ .

in time for decay from a fixed  $l_{\text{flight}}$  with increasing  $T_B$ .

The cross section and relative population for the  $5\text{p}^2\text{P}_{3/2}$  ( $2212.6 \text{ cm}^{-1}$ ) state in indium has a different behaviour, as the  $5\text{p}^2\text{P}_{3/2}$  state is far off resonance with the IP of sodium, then the effective broadening of the resonance in Fig. 1 with increasing beam energy is the route to its population, which is shown in Fig. 2. Therefore the relative population of the  $5\text{p}^2\text{P}_{3/2}$  state in indium decreases with increasing beam energy,  $T_B$ , as the population of the nearby  $5\text{p}^2\text{P}_{1/2}$  state and many higher-lying states begins to compete. One has to balance these factors when choosing a combination of electron donor element and beam energy to maximise the population of the atomic state of interest in the product atomic beam.

### 3. Experimental method

The measurements in this paper were performed using the collinear resonance ionization spectroscopy (CRIS) beamline [50,51] at CERN-ISOLDE [3]. Fig. 3 shows the layout of the experimental setup. A solid

target of indium of 99% purity was used to produce the indium ions for the experiment by means of laser ablation [1].

A pulsed 532-nm laser beam from a Litron LPY 601 50–100 PIV Nd:YAG laser was focused to a fluence of  $> 0.5 \text{ J/cm}^2$  onto the target surface at an angle of  $45^\circ$ , creating a pulsed plasma of indium ions at a repetition rate of 100 Hz. A series of electrostatic ion optics then accelerated the  $\text{In}^+$  ions to 20 keV and guided them through a  $34^\circ$  bend to be collinearly overlapped with two laser beams. The ions were then neutralised with a sodium filled charge-exchange cell heated to  $300(10)^\circ\text{C}$ . The remaining ion fraction was electrostatically deflected after the cell.

After 120 cm of flight the atomic populations were then probed by the atomic transitions  $5\text{p}^2\text{P}_{1/2} \rightarrow 8\text{s}^2\text{S}_{1/2}$  at  $40506.421 \text{ cm}^{-1}$  (246.0 nm) and  $5\text{p}^2\text{P}_{3/2} \rightarrow 9\text{s}^2\text{S}_{1/2}$  at  $40636.98 \text{ cm}^{-1}$  (246.8 nm), for the ground and metastable states respectively. The second head of the same Nd:YAG laser at a wavelength of 1064 nm was then used to non-resonantly ionize the excited atom. A laser fluence of  $120 \text{ mJ/cm}^2$  was measured at the entrance of the beamline for the 1064-nm light, when on resonance no decrease in count rate was observed outside of experimental scatter down by 80%. It was assumed that differences in the non-resonant ionization probabilities from the upper states of the 246.0-nm and 246.8-nm transitions ( $8\text{s}^2\text{S}_{1/2}$  and  $9\text{s}^2\text{S}_{1/2}$  respectively) were compensated by the high pulse energy of the non-resonant 1064-nm laser. The laser was delayed by  $\sim 20 \text{ ns}$  from the resonant excitation step to avoid lineshape distortions from the high-power pulsed light [51]. These laser-ionization pathways are shown in Fig. 4. The ions were then deflected through  $20^\circ$  and counted by a micro-channel plate (MCP) detector (MCP).

The resonant-step laser light was produced using a injection-locked Ti:Sapphire laser [52,53] seeded using a narrowband SolsTiS continuous-wave Ti:Sapphire laser by M-Squared and pumped using a LEE LDP-100MQ Nd:YAG laser. With this laser system, pulsed narrowband laser light (1 kHz repetition rate) was produced at  $13545.66 \text{ cm}^{-1}$  (740 nm) or  $13,502.14 \text{ cm}^{-1}$  (738 nm). This light was then frequency tripled to  $40,636.98 \text{ cm}^{-1}$  (246.8 nm) and  $40,506.421 \text{ cm}^{-1}$  (246.0 nm) by the use of non-linear  $\text{BiB}_3\text{O}_6$  and  $\text{BaB}_2\text{O}_4$  crystals [54]. A laser fluence of  $15(1) \mu\text{J}/\text{cm}^2$  was used for both transitions, measured at the entrance of the beamline, which is well above a saturation threshold of  $5(2) \mu\text{J}/\text{cm}^2$  measured with the same setup for the 246.8-nm transition. The greater laser fluence was used to reduce susceptibility to fluctuations in laser power. A laser beam waist of approximately 8 mm was measured at the laser-atom interaction region for the 1064-nm light, and 10 mm for the 246.8-nm and 246.0-nm light. The ablation ion source provided the ideal pulsed time structure, time synchronisation and high ion density needed for efficient overlap with the pulsed lasers without the use of cooling and bunching [55] typically needed for CRIS.

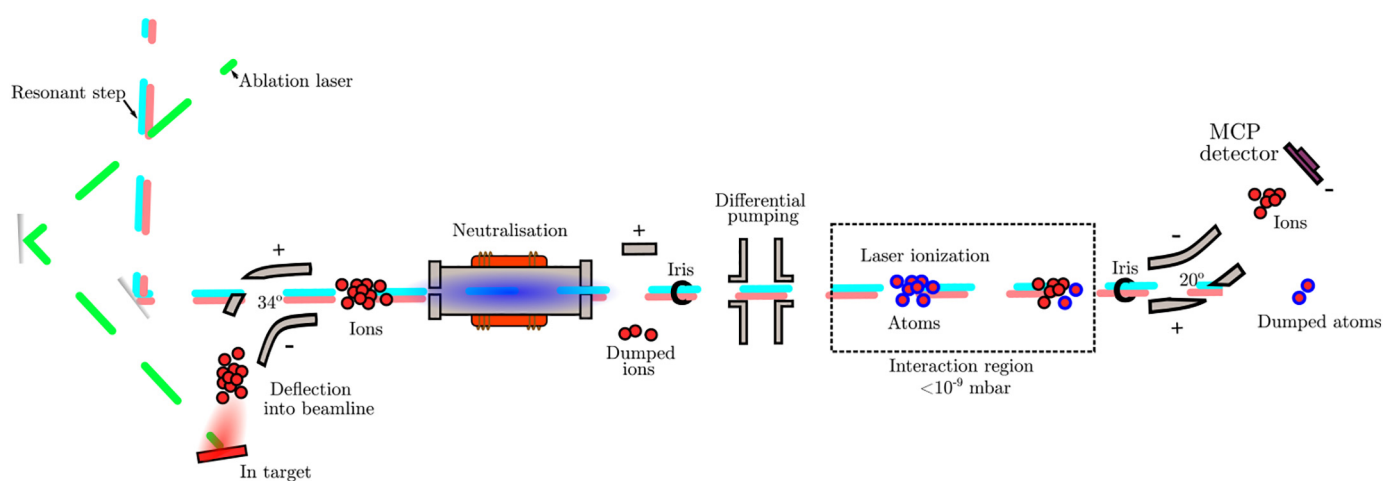


**Fig. 3.** Simplified schematic of the collinear resonance ionization spectroscopy set-up used to make the population measurements.

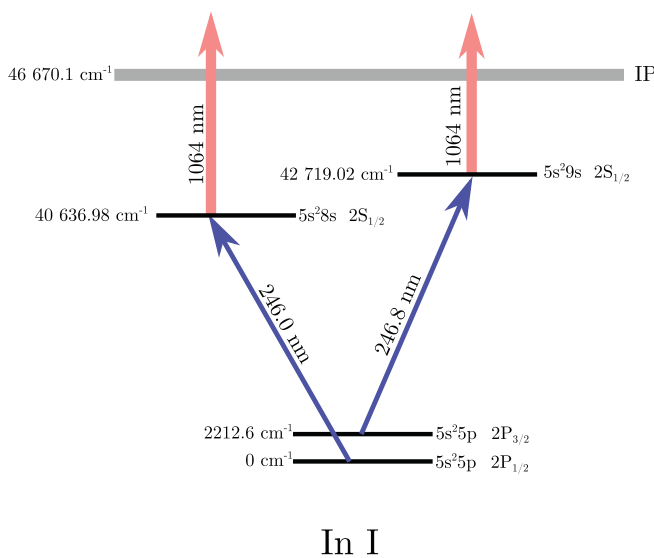


**Fig. 4.** Laser ionization scheme used to probe the indium ground and metastable state populations,  $5p\ ^2P_{1/2}$  and  $5p\ ^2P_{3/2}$ .

It is worth noting that pulsed laser light can typically reduce pumping to dark states compared to cw laser light, depending upon the relevant transitions of the element of interested [56,57], which is especially important in relative population measurements as the populations would be altered. Further details of this source and the CRIS setup can be found in [1].

Due to the close proximity of the two transitions, they could quickly be switched between and near identical laser beam properties between the two measurements could be maintained. Spatial overlap of the atoms and ions was ensured by alignment irises and Faraday cups through which both laser and ion beam transport was maximised. The ion beam waist was measured to be  $< 4$  mm by the irises. The integrated count rate of a hyperfine spectrum scan was used for each transition to give the relative proportion of the atomic population in the  $5p\ ^2P_{1/2}$  and  $5p\ ^2P_{3/2}$  states. Normalisation for variation in atom beam intensity was included using the collisional re-ionization background count rate.

#### 4. Results and discussion

##### 4.1. Relative populations

The populations measured in this work as well as the results of the simulation are displayed in Table 1. Since the populations are relative, the ratio of the states was used for comparison to simulation, which introduces the error in the calculated value reported for the  $5p\ ^2P_{3/2}$  state. The experimental uncertainty was obtained using the statistical error from the integrated counts of the hyperfine spectra, in addition to

the uncertainty in the background count rate used to normalised the neutral beam current. Although the experimental error is large the relative populations were well reproduced and give confidence in extending the method to other atomic systems. This will provide valuable quantification of the expected useful neutral fraction in similar CLS experiments. The simulations will also be compared against the only available relative atomic population data, for fluorine and nickel.

The normalisation performed was using the non-resonant background count rate of the spectra which has a large uncertainty for small measurement times. In future studies, potential systematic errors of the method could be quantified and corrected for by measuring the instantaneous number of discarded atoms of each atom bunch, using an atom detector [59,60]. Laser intensities will then also simultaneously be recorded with a photodiode. It is expected that using this combined information to normalize variations in beam current and laser light intensities will create an effective experimental setup for measuring relative atomic populations following charge exchange.

**Table 1** shows a comparison of the R&F simulation method with the few known measurements of relative populations following neutralisation. To the authors knowledge this table displays all relative population measurements available to-date for beam energies of  $T_B = 1\text{--}100$  keV. The ratio of the simulated to the experimental values for fluorine is a factor of 2. The initial relative population of the state of interest is 0.079 however, which is within the uncertainty of the experiment. It could be that the high-lying contributions which decay to this state were collisionally ionized before decaying, or that the transition rates of these states were overestimated in literature. Alternatively the difference could be due to underestimated experimental uncertainties, arising from the preferential ionization [61] factor used by [58] in the calculation of the population or neglected experimental factors. Despite this the magnitude is well reproduced given the assumptions that were made to extract the population.

The relative populations are in good agreement with the measured populations for nickel. Surprisingly, no population above background was observed for the  $4s^3D_1$  state measurements performed by [45] using the strong ( $A_{ij} = 1.2 \times 10^8 s^{-1}$ )  $4s^3D_1 \rightarrow 4p^3P_0$  transition. An initial population of 0.033 was simulated for the  $4s^3D_1$  state, while background fluctuations placed an upper limit of  $< 0.013$  on the population they measured. One explanation could be inaccurate branching ratios of the transitions de-exciting the initial population, which would reduce the population of the  $4s^3D_1$  state.

As the calculation method has proven to be useful in predicting relative populations in these cases, the calculations have been extended to all elements from  $Z = 1$  to  $Z = 89$  with available atomic data, for incident ions  $A^+(0)$  upon potassium and sodium vapours  $B(0)$



where both the vapour and ion beam are again assumed to be in their ground states. The results are shown in Tables 2 and 3 for potassium and sodium vapours respectively.

It is worth noting that carbon and oxygen are predicted to have a large population in metastable states following charge exchange. These

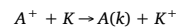
**Table 1**

Comparison of available experimental data to simulation of relative populations following neutralisation. \* - experimental populations were taken relative to these states. Abbreviations: Sim. Rel. Pop. - Simulated Relative Population, Ini. - Initial, Fin. - Final, Exp. - Experiment.

$T_B$ (keV)	$l_{\text{flight}}$ (cm)	State	Sim. Rel. Pop.		Exp.	Sim. Rel. Pop. [45]
			Ini.	Fin.		
In	20	$5p^2P_{1/2}$	0.314	0.319	*	
In	20	$5p^2P_{3/2}$	0.664	0.665	0.619(116)	
F	40.8	$3s^4P_{5/2}$	0.079	0.19	0.083(4) [58]	
Ni	29.85	$4s^3D_3$	0.025	0.130	*	
Ni	29.85	$4s^3D_2$	0.028	0.107	0.114(10) [45]	0.1138(100)
Ni	29.85	$4s^3D_1$	0.033	0.06	< 0.013 [45]	0.083(1)
Ni	29.85	$4s^1D_2$	0.015	0.02435	0.0229(46) [45]	0.0354(1)

**Table 2**

Atomic population distribution simulation results for neutralisation of an ion beam of elements A = 1–90 by free K atoms. Atomic data sourced from the NIST atomic database[48]. Only the 5 most populous states are listed in this table. † - insufficient transition data was available to provide reliable values for these elements. ‡ - insufficient level data was available for these elements. \* - these light elements are outside of the intermediate velocity region at 40 keV. The columns for 0 cm and 120 cm flight distance give respectively the initial populations after charge exchange at 0 cm and the final populations after a further 120 cm of atom flight at the corresponding beam energy.



$40 \text{ keV}$									$5 \text{ keV}$										
$A^+$			Initial (0.0 cm)			Final (120.0 cm)			Initial (0.0 cm)			Final (120.0 cm)							
(Z)	#	Level ( $\text{cm}^{-1}$ )	%	Level ( $\text{cm}^{-1}$ )	%	Level ( $\text{cm}^{-1}$ )	%	Level ( $\text{cm}^{-1}$ )	%	Level ( $\text{cm}^{-1}$ )	%	Level ( $\text{cm}^{-1}$ )	%	Level ( $\text{cm}^{-1}$ )	%	Level ( $\text{cm}^{-1}$ )	%		
1*	1	107,965.04916	1	0.0	41.5	82,258.91911	4.4	0.0	60.8	1*	2	107,965.04971	1	82,258.9544	4.4	82,258.9544	4.9		
	3	107,965.05487	1	107,440.43933	1	82,259.158	4.4	107,440.4385	0.8		4	107,965.05488	1	82,259.285	4.4	107,440.43933	0.8		
	5	107,965.05677	1	108,324.72416	1	97,492.2112	1.8	107,965.04916	0.7		1	166,277.44014	1.2	159,855.97433	16.4	159,855.97433	75.8		
	2	169,086.76647	1.2	0.0	9.1	166,277.44014	10.4	0.0	7		3	169,086.8429	1.2	169,086.76647	7.5	166,277.44014	4.3		
	4	169,087.83081	1.2	193,921.61772	0.7	169,086.8429	7.5	193,921.61772	0.3		5	159,855.97433	1.2	169,087.83081	7.5	193,921.61772	0.3		
3*	1	0.0	4.4	0.0	52.5	0.0	53.2	0.0	90.2	3*	2	14,903.66	4.1	42,003.3	0.7	14,903.66	12.5	42,003.3	0.2
	3	14,904.0	4.1	42,298.0	0.7	14,904.0	12.5	42,298.0	0.1		4	27,206.12	2.4	42,389.0	0.7	27,206.12	1.4	42,389.0	0.1
	5	30,925.38	1.8	42,389.0	0.7	30,925.38	0.7	42,389.0	0.1		1	42,565.35	4.2	21,978.28	64.2	21,978.28	44.8		
	2	21,981.27	3.1	21,978.925	15.5	21,981.27	15.0	21,978.925	21.6		3	21,978.925	3.1	0.0	6.3	21,981.27	18.2		
	4	21,978.28	3.1	21,981.27	5.9	21,978.28	15.0	0.0	13		5	52,080.94	2.9	56,882.43	1.6	56,882.43	0.8		
4	1	28,647.43	7	0.0	37.1	28,647.43	30.6	28,647.43	30.6	4	2	28,652.07	7	15.287	14.4	28,652.07	30.5		
	3	28,658.4	7	28,647.43	6.9	28,658.4	30.5	28,658.4	30.5		4	40,039.6907	5.2	28,652.07	6.9	40,039.6907	2.6		
	5	47,856.809	3.2	28,658.4	6.9	15.287	0.5	15.287	1.3		1	60,333.43	2.2	16.4	36.7	60,333.43	48.3		
	2	60,352.63	2.1	0.0	21.1	60,352.63	11.7	0.0	29.2		3	60,393.14	2.1	43.4	13.4	60,393.14	9.2		
	4	61,981.82	2	10,192.63	6	61,981.82	7.9	10,192.63	5.6		5	64,086.92	1.8	33,735.2	0.8	33,735.2	2.6		
5	1	83,284.07	2.4	0.0	54.7	83,284.07	16.2	0.0	82.8	5	2	83,317.83	2.4	19,224.464	8	83,317.83	16.0		
	3	83,364.62	2.4	19,224.464	5.1	83,364.62	15.8	19,224.464	6.1		4	86,137.35	2.2	19,233.177	5.1	19,233.177	5.6		
	5	86,220.51	2.2	28,838.92	1.1	86,137.35	7.5	28,838.92	0.2		1	73,768.2	6.1	46.8	46.8	73,768.2	72.3		
	2	76,794.978	5.5	0.0	19.9	76,794.978	23.1	0.0	21.8		3	86,625.757	2.7	158,265	4.1	86,625.757	1.1		
	4	86,627.778	2.7	102,865.655	0.9	86,627.778	1.5	102,865.655	0.1		5	86,631.454	2.7	226,977	0.7	86,631.454	0.1		
6	1	102,405.71	6	102,405.71	19.1	102,405.71	23.4	102,405.71	29.8	6	2	102,680.44	6	102,680.44	22.0	102,680.44	27		
	3	102,840.38	6	102,840.38	10.8	102,840.38	21.2	102,840.38	24.9		4	104,731.05	5.7	104,731.05	12.8	104,731.05	8.2		
	5	105,056.28	5.6	105,056.28	5.1	105,056.28	11.7	105,056.28	6.9		1	134,041.84	6.6	0.0	25.2	134,041.84	44.9		
	2	134,459.2871	6.6	134,041.84	22.1	134,459.2871	24.9	134,041.84	33.4		3	134,818.6405	6.6	134,818.6405	23.5	134,818.6405	18.6		
	4	135,888.7173	6.5	158,601.1152	2	135,888.7173	18.9	158,601.1152	0.1		5	148,257.7898	2.7	159,379.9935	0.8	159,379.9935	0.1		
7	1	0.0	26.4	0.0	72.9	0.0	95.5	0.0	98.8	7	2	16,956.17025	8.4	37,059.54	0.5	16,956.17025	0.8		
	3	16,973.36619	8.4	38,400.9	0.4	16,973.36619	0.8	38,400.9	0		4	25,739.999	2.5	38,400.904	0.4	38,400.904	0		
	5	29,172.837	1.5	38,401.147	0.4	29,172.837	0.1	38,401.147	0		1	21,850.405	13.4	21,870.464	27.8	21,850.405	33.3		
	2	21,870.464	13.4	21,850.405	26	21,870.464	32.5	21,870.464	33		3	21,911.178	13.4	21,911.178	22	21,911.178	32.7		
	4	35,051.264	5.3	0.0	6.3	35,051.264	0.5	0.0	0.4		5	0.0	2.9	46,403.065	2.3	46,403.065	0.1		
12	1	112,061	18.4	0.0	41.5	112,061	46.9	0.0	48.6	12	2	0.0	18.3	112,061	30.3	45.1	112,061	48	
	3	25,347.756	5.8	29,020.41	3.5	25,347.756	1.2	29,020.41	0.6		4	29,020.41	3.5	29,066.96	3.5	29,066.96	0.5		
	1	112,061	18.4	0.0	41.5	112,061	46.9	0.0	48.6		2	0.0	18.3	112,061	30.3	45.1	112,061	48	
	3	25,347.756	5.8	29,020.41	3.5	25,347.756	1.2	29,020.41	0.6		4	29,020.41	3.5	29,066.96	3.5	29,066.96	0.5		

(continued on next page)

**Table 2** (continued)

$A^+ + K \rightarrow A(k) + K^+$										
40 keV										
$A^+$		Initial (0.0 cm)			Final (120.0 cm)			5 keV		
(Z)	#	Level (cm <sup>-1</sup> )	%	Level (cm <sup>-1</sup> )	%	Level (cm <sup>-1</sup> )	%	Level (cm <sup>-1</sup> )	%	
14	5	29,066.96	3.5	29,142.78	3.4	29,066.96	0.5	29,142.78	0.5	
	1	33,326.053	8.5	77.115	27.9	15,394.37	32.8	33,326.053	25	
	2	15,394.37	7.6	0.0	22.6	33,326.053	27.6	77.115	24.4	
	3	39,683.163	4.2	223.157	8.3	39,683.163	3.5	0.0	18.3	
	4	39,760.285	4.2	6298.85	5.3	39,760.285	3.4	15,394.37	7.6	
15	5	39,955.053	4	33,326.053	5.2	39,955.053	3.2	223.157	5.7	
	1	55,939.421	4.2	0.0	30	55,939.421	9.9	0.0	50.6	
	2	56,090.626	4.1	11,361.02	6.5	56,090.626	9.5	11,361.02	8.4	
	3	56,339.656	4	65,788.455	1.9	56,339.656	8.7	65,788.455	1.4	
	4	57,876.574	3.3	65,585.13	1.9	57,876.574	5.5	65,585.13	1.4	
16	5	58,174.366	3.2	65,450.125	1.9	58,174.366	5.1	65,450.125	1.4	
	1	52,623.64	10.8	0.0	38.5	52,623.64	36.5	0.0	47.6	
	2	55,330.811	7.8	52,623.64	32.1	55,330.811	14.9	52,623.64	31.7	
	3	22,179.954	3.5	63,446.065	13.6	22,179.954	4.3	63,446.065	8	
	4	63,446.065	2.6	396.055	6.9	63,446.065	1.9	396.055	8	
17	5	63,457.142	2.6	573.64	2.6	63,457.142	1.9	573.64	1.3	
	1	71,958.363	7.7	0.0	42.4	71,958.363	22.5	0.0	67.2	
	2	72,488.568	7.3	71,958.363	12.2	72,488.568	18.3	882.3515	17.1	
	3	72,827.038	7	882.3515	12.1	72,827.038	16.1	71,958.363	6.1	
	4	74,225.846	5.9	87,979.49	1.1	74,225.846	9.7	87,979.49	0.4	
18	5	74,865.667	5.4	88,080.042	1.1	74,865.667	7.8	88,080.042	0.4	
	1	93,143.76	11.3	0.0	29.3	93,143.76	30.0	93,143.76	40.8	
	2	93,750.5978	10.5	93,143.76	28.6	93,750.5978	22.9	0.0	36.6	
	3	94,553.6652	9.5	94,553.6652	9.6	94,553.6652	16.1	94,553.6652	12.8	
	4	95,399.8276	8.5	112,750.153	1.1	95,399.8276	11.4	112,750.153	0.3	
19	5	104,102.099	2.1	113,716.555	0.9	104,102.099	0.8	113,716.555	0.3	
	1	0.0	36.5	0.0	65.5	0.0	87.8	0.0	94	
	2	12,985.18572	5.4	30,617.31	0.4	12,985.18572	1.2	30,617.31	0.1	
	3	13,042.89603	5.4	30,617.31	0.4	13,042.89603	1.1	30,617.31	0.1	
	4	21,026.551	1.5	33,910.42	0.3	21,026.551	0.3	33,910.42	0	
20	5	21,534.68	1.4	33,910.42	0.3	21,534.68	0.3	33,910.42	0	
	1	15,157.901	10.3	15,210.063	14.9	15,157.901	21.2	15,157.901	25.8	
	2	15,210.063	10.2	15,157.901	14.4	15,210.063	20.7	15,210.063	24.8	
	3	15,315.943	10.1	15,315.943	14	15,315.943	19.7	15,315.943	23.9	
	4	0.0	8.7	20,335.36	9.3	0.0	18.7	0.0	8.5	
21	5	20,335.36	5.1	20,349.26	8.3	20,335.36	2.7	20,335.36	4	
	1	11,677.38	3.3	0.0	12.3	11,519.99	11.8	11,519.99	13.9	
	2	11,610.28	3.3	168.34	10.6	11,557.69	11.8	11,557.69	13.9	
	3	11,557.69	3.3	11,519.99	6.2	11,610.28	11.8	11,610.28	13.9	
	4	11,519.99	3.3	11,557.69	5.7	11,677.38	11.8	11,677.38	13.9	
22	5	14,926.07	3	11,610.28	5.6	14,926.07	4.6	0.0	8.5	
	1	14,105.634	1.4	0.0	6	13,981.773	5.3	15,877.081	5.4	
	2	14,028.436	1.4	386.874	5.2	14,028.436	5.3	16,106.076	4.9	
	3	13,981.773	1.4	170.1328	4.9	14,105.634	5.2	15,975.631	4.7	
	4	15,108.111	1.4	6598.765	4.3	15,108.111	4.3	15,108.111	4.2	
23	5	15,156.802	1.4	6742.756	3.8	15,156.802	4.3	15,156.802	4.2	
	1	13,801.54	1.3	2153.21	6.2	13,801.54	4.7	14,909.97	4.1	
	2	13,810.94	1.3	2220.11	5.6	13,810.94	4.7	14,949.37	4	
	3	14,514.76	1.3	2311.36	4.9	14,514.76	3.9	15,000.94	3.9	
	4	14,548.81	1.3	2112.28	4.3	14,548.81	3.9	15,062.96	3.9	
24	5	14,909.97	1.3	2424.78	4.2	11,100.59	3.4	2220.11	3.4	
	1	8307.5753	2.8	0.0	11.5	8307.5753	11.1	8307.5753	11.4	
	2	8095.1842	2.8	7593.1484	6.6	8095.1842	10.0	8095.1842	10.4	
	3	7927.441	2.7	7810.7795	4.2	7927.441	9.2	7927.441	9.6	
	4	7810.7795	2.7	7927.441	4.2	7810.7795	8.7	7593.1484	9.4	
25	5	7750.7465	2.7	8095.1842	4.1	7750.7465	8.5	7810.7795	9.1	
	1	18,705.37	4.3	0.0	13.6	18,531.64	11.9	18,705.37	14.6	
	2	18,531.64	4.3	18,402.46	6.8	18,705.37	11.8	18,402.46	13.8	
	3	18,402.46	4.3	18,705.37	6.6	18,402.46	11.8	18,531.64	13.5	
	4	17,637.15	4.2	18,531.64	6.4	17,637.15	10.7	17,637.15	9.9	
26	5	17,568.48	4.2	17,451.52	5.6	17,568.48	10.5	17,568.48	9.8	
	1	22,650.416	1.3	0.0	8	22,249.429	3.2	22,650.416	5.4	
	2	22,838.323	1.3	415.933	6.2	22,650.416	3.2	23,270.384	5	
	3	22,845.869	1.3	704.007	5.8	21,999.13	3.2	0.0	4.4	
	4	22,946.816	1.3	888.132	4.7	22,838.323	3.1	23,244.838	4.3	
27	5	22,996.674	1.3	19,350.891	2.4	22,845.869	3.1	23,192.5	4.1	
	1	22,475.36	2	0.0	7.7	21,920.09	6.4	23,611.78	9.1	
	2	23,152.57	2	816.0	5.9	22,475.36	6.4	23,855.62	8.3	
	3	21,920.09	2	1406.84	4.7	21,780.47	6.4	24,326.11	6.8	

(continued on next page)

**Table 2** (continued)

$A^+ + K \rightarrow A(k) + K^+$									
40 keV									
$A^+$	Initial (0.0 cm)			Final (120.0 cm)			5 keV		
(Z)	#	Level ( $\text{cm}^{-1}$ )	%	Level ( $\text{cm}^{-1}$ )	%	Level ( $\text{cm}^{-1}$ )	%	Level ( $\text{cm}^{-1}$ )	%
28	4	23,184.23	2	1809.33	3.6	21,215.9	5.8	24,733.28	5.6
	5	23,207.76	2	23,611.78	3.6	23,152.57	5.7	25,041.16	4.7
	1	22,102.325	4.5	204,787	16	22,102.325	32.6	22,102.325	16.5
	2	16,017.306	3.5	0.0	13.7	16,017.306	10.3	0.0	11.5
	3	15,734.001	3.4	879.816	12.1	15,734.001	8.8	16,017.306	9.3
29	4	15,609.844	3.4	1713.087	6.6	15,609.844	8.2	25,753.553	9
	5	25,753.553	3.3	1332.164	5	14,728.84	5.1	204.787	8.7
	1	13,245.443	18.8	0.0	39.9	13,245.443	41.7	13,245.443	41.8
	2	30,535.324	14	13,245.443	19.2	11,202.618	17.8	0.0	31.7
	3	11,202.618	13.5	11,202.618	16.7	30,535.324	14.3	11,202.618	18.9
30	4	30,783.697	13.4	39,018.69	2.7	30,783.697	12.9	39,018.69	1
	5	39,018.69	2.7	40,909.16	1.9	39,018.69	1.0	40,909.16	0.7
	1	32,890.352	27.1	32,890.352	29.4	32,890.352	37.8	32,890.352	37.9
	2	32,501.421	26.4	32,501.421	28.7	32,501.421	32.2	32,501.421	32.3
	3	32,311.35	26.1	32,311.35	28.4	32,311.35	29.5	32,311.35	29.6
31	4	46,745.413	5.5	46,745.413	2	46,745.413	0.2	46,745.413	0.1
	5	53,672.28	1.4	53,672.28	1.5	53,672.28	0.0	53,672.28	0
	1	826.19	39.7	826.19	41.6	826.19	58.0	826.19	58.2
	2	0.0	34.7	0.0	40.2	0.0	37.8	0.0	38.8
	3	24,788.53	3.9	33,044.05	0.8	24,788.53	0.7	33,044.05	0.1
32	4	33,044.05	0.8	33,155.07	0.8	33,044.05	0.1	33,155.07	0.1
	5	33,155.07	0.8	37,975.768	0.4	33,155.07	0.1	37,975.768	0.1
	1	16,367.3332	39.9	557.1341	28.3	16,367.3332	83.5	16,367.3332	42.6
	2	7125.2989	7.3	0.0	18.6	7125.2989	2.4	557.1341	17.8
	3	37,451.6893	6	16,367.3332	8.8	37,451.6893	1.7	0.0	12
33	4	37,702.3054	5.7	1409.9609	7.5	37,702.3054	1.6	1409.9609	4.6
	5	39,117.9021	4.1	7125.2989	4.9	39,117.9021	1.1	7125.2989	3.7
	1	50,693.8	12.2	50,693.8	16.1	50,693.8	14.1	50,693.8	18.4
	2	51,610.2	9.8	51,610.2	13	51,610.2	10.7	51,610.2	13.9
	3	52,897.9	7.3	52,897.9	9.6	52,897.9	7.4	52,897.9	9.7
34 <sup>†</sup>	4	53,135.6	6.9	55,366.4	5.5	53,135.6	7.0	55,366.4	5.2
	5	54,605.3	4.9	53,135.6	4.6	18,647.5	5.0	53,135.6	4.6
	1	48,182.19	24.1			48,182.19	33.4		
	2	50,996.931	12.2			22,446.202	13.7		
	3	22,446.202	11.9			50,996.931	12.6		
35	4	59,242.798	1.9			59,242.798	1.6		
	5	59,287.818	1.9			59,287.818	1.5		
	1	63,436.45	19.7	63,436.45	23.8	63,436.45	30.6	63,436.45	35.4
	2	64,907.19	13.9	64,907.19	16.8	64,907.19	17.0	64,907.19	19.7
	3	66,883.87	8.6	66,883.87	10.4	66,883.87	8.5	66,883.87	9.8
36	4	67,183.58	8	67,183.58	4.8	67,183.58	7.7	67,183.58	4.4
	5	68,970.21	5.2	68,970.21	3.1	68,970.21	4.4	68,970.21	2.6
	1	79,971.7417	23.5	79,971.7417	30.2	79,971.7417	36.6	79,971.7417	42.6
	2	80,916.768	18.8	80,916.768	22.6	80,916.768	23.7	80,916.768	26.3
	3	85,191.6166	6.6	85,191.6166	5.5	85,191.6166	5.1	85,191.6166	4.1
37	4	85,846.7046	5.6	85,846.7046	5.1	85,846.7046	4.3	85,846.7046	3.6
	5	91,168.515	1.6	91,168.515	1.5	91,168.515	1.2	91,168.515	1
	1	0.0	58.5	0.0	63.3	0.0	79.6	0.0	82.3
	2	12,578.95	3	12,816.545	3.2	12,578.95	1.6	12,816.545	1.6
	3	12,816.545	2.9	19,355.203	0.9	12,816.545	1.5	19,355.203	0.5
38	4	19,355.203	0.9	19,355.649	0.9	19,355.203	0.5	19,355.649	0.5
	5	19,355.649	0.9	20,132.51	0.8	19,355.649	0.5	20,132.51	0.4
	1	0.0	33.9	0.0	20.1	0.0	82.4	0.0	66.7
	2	14,317.507	11.6	14,317.507	17.3	14,317.507	3.9	14,317.507	9.3
	3	14,504.334	11.1	14,898.545	14.4	14,504.334	3.6	14,898.545	7.1
39	4	14,898.545	10.1	14,504.334	13.5	14,898.545	3.1	14,504.334	4.9
	5	18,159.04	4.5	18,159.04	7.8	18,159.04	1.0	18,159.04	2.9
	1	10,529.169	6.1	0.0	6.7	10,529.169	20.5	10,529.169	20.5
	2	10,937.39	5.9	10,937.39	6.2	10,937.39	15.9	10,937.39	16
	3	11,078.614	5.8	10,529.169	6.1	11,078.614	14.5	11,078.614	14.5
40 <sup>†</sup>	4	11,277.928	5.7	11,078.614	5.9	11,277.928	12.7	11,277.928	12.7
	5	11,359.757	5.6	11,277.928	5.9	11,359.757	12.0	11,359.757	12
	1	12,342.37	2.2			11,956.33	7.7		
	2	12,503.44	2.2			12,342.37	7.6		
	3	11,956.33	2.2			12,503.44	7.5		
41 <sup>†</sup>	4	12,760.66	2.2			11,640.72	7.4		
	5	12,772.78	2.2			12,760.66	7.0		
	1	13,404.77	1.7			13,145.71	4.7		
	2	13,145.71	1.7			13,012.2	4.7		

(continued on next page)

**Table 2** (continued)

$A^+ + K \rightarrow A(k) + K^+$									
40 keV									
$A^+$	Initial (0.0 cm)			Final (120.0 cm)			5 keV		
(Z)	#	Level ( $\text{cm}^{-1}$ )	%	Level ( $\text{cm}^{-1}$ )	%	Level ( $\text{cm}^{-1}$ )	%	Level ( $\text{cm}^{-1}$ )	%
42	3	13,515.2	1.7			12,982.38	4.7		
	4	13,629.15	1.7			13,404.77	4.6		
	5	13,012.2	1.7			12,692.12	4.6		
	1	16,641.081	3.3	0.0	5.2	16,641.081	12.8	16,641.081	13.1
	2	16,692.905	3.3	16,692.905	3.9	16,692.905	12.5	16,692.905	12.9
43	3	16,747.72	3.3	16,747.72	3.9	16,747.72	12.2	16,747.72	12.6
	4	16,783.856	3.3	16,641.081	3.9	16,783.856	12.1	16,783.856	12.4
	5	16,784.522	3.3	16,783.856	3.9	16,784.522	12.1	16,784.522	12.4
	1	16,287.79	2.4	16,428.71	4.7	16,025.15	6.1	16,428.71	10.4
	2	16,133.98	2.4	16,874.51	4.7	16,133.98	6.1	16,874.51	9.1
44	3	16,025.15	2.4	17,522.92	4.6	15,770.42	6.1	17,522.92	6.6
	4	16,415.64	2.4	0.0	4.5	16,287.79	6.0	16,025.15	5.4
	5	16,428.71	2.4	16,287.79	2.4	15,624.25	5.9	16,133.98	5.4
	1	17,096.87	2.8	0.0	3.5	17,096.87	12.6	17,096.87	18.6
	2	17,045.97	2.8	17,096.87	3.2	17,045.97	12.3	16,240.13	12
45	3	16,712.58	2.8	16,240.13	3	16,712.58	10.6	16,712.58	11.2
	4	16,240.13	2.7	15,550.16	2.8	16,240.13	8.1	16,190.61	8.3
	5	20,055.71	2.7	1190.64	2.6	16,190.61	7.8	15,550.16	7.6
	1	16,943.5	6.9	16,943.5	11.3	16,943.5	26.4	16,943.5	36.7
	2	16,120.72	6.3	16,118.69	10.3	16,120.72	15.0	16,118.69	20.8
46	3	16,118.69	6.3	0.0	9.4	16,118.69	15.0	16,120.72	10.4
	4	16,017.94	6.2	14,787.87	8.4	16,017.94	13.9	16,017.94	9.6
	5	14,787.87	5.2	12,723.07	5.7	14,787.87	5.7	14,787.87	7.9
	1	25,101.235	20.3	25,101.235	25.2	25,101.235	62.9	25,101.235	63.6
	2	28,213.767	18.3	28,213.767	22.7	28,213.767	27.0	28,213.767	27.3
47	3	29,711.109	14.7	29,711.109	18.2	29,711.109	7.5	29,711.109	7.5
	4	34,068.977	5.5	6564.148	8.4	34,068.977	0.5	6564.148	0.4
	5	35,041.751	4.3	34,068.977	3.7	35,041.751	0.3	34,068.977	0.3
	1	29,552.05741	29.6	0.0	59.1	29,552.05741	34.8	0.0	62.9
	2	30,242.29835	24.7	30,242.29835	24.7	30,242.29835	26.2	30,242.29835	26.2
48	3	30,472.66516	23.2	34,714.22643	7.9	30,472.66516	23.9	34,714.22643	5.7
	4	34,714.22643	7.9	42,556.147	1.5	34,714.22643	5.7	42,556.147	0.9
	5	0.0	4.3	51,886.965	0.3	0.0	2.9	51,886.965	0.2
	1	31,826.952	31.8	31,826.952	32.7	30,656.087	36.4	0.0	36.3
	2	30,656.087	31.7	30,113.99	32	31,826.952	33.6	31,826.952	33.7
49	3	30,113.99	30.8	0.0	28.5	30,113.99	29.9	30,113.99	29.9
	4	43,692.384	2.4	30,656.087	5.1	43,692.384	0.0	30,656.087	0.2
	5	51,483.98	0.4	58,390.9	0.1	51,483.98	0.0	53,310.101	0
	1	2212.599	56.8	2212.599	57.1	2212.599	83.3	2212.599	83.4
	2	0.0	36.9	0.0	38.3	0.0	16.2	0.0	16.3
50	3	24,372.957	1	31,816.982	0.2	24,372.957	0.1	31,816.982	0
	4	31,816.982	0.2	32,115.251	0.2	31,816.982	0.0	32,115.251	0
	5	32,115.251	0.2	34,977.678	0.2	32,115.251	0.0	34,977.678	0
	1	17,162.499	67.5	17,162.499	26.1	17,162.499	99.1	17,162.499	95.4
	2	8612.955	12.4	1691.806	15.7	8612.955	0.4	8612.955	1.3
51	3	3427.673	3.5	8612.955	14.5	3427.673	0.1	1691.806	0.9
	4	1691.806	2.4	3427.673	13.9	1691.806	0.1	3427.673	0.8
	5	0.0	1.7	0.0	11.4	0.0	0.0	0.0	0.7
	1	18,464.202	35.9	18,464.202	29.5	18,464.202	46.4	18,464.202	39.9
	2	16,395.359	21.2	0.0	19.1	16,395.359	21.6	16,395.359	18.5
52	3	43,249.337	6.3	16,395.359	17.5	43,249.337	5.0	0.0	15.7
	4	9854.018	4.8	9854.018	5.5	9854.018	3.8	9854.018	4.5
	5	8512.125	3.6	8512.125	5.4	8512.125	2.9	8512.125	4.5
	1	23,198.392	50.3	0.0	30.8	23,198.392	69.4	23,198.392	37.2
	2	44,253.0	11	23,198.392	21	44,253.0	7.5	0.0	26.8
53	3	46,652.738	5.7	54,160.094	2.2	46,652.738	3.6	54,160.094	1.7
	4	10,557.877	2.7	54,199.122	2.1	10,557.877	1.7	54,199.122	1.7
	5	4750.712	1.1	54,535.345	2	4750.712	0.7	54,535.345	1.6
	1	54,633.46	20.8	0.0	36.2	54,633.46	24.5	0.0	41.2
	2	56,092.881	13.6	7602.97	5	56,092.881	14.8	7602.97	5
54	3	60,896.243	3.8	63,186.758	2.4	60,896.243	3.8	63,186.758	2.4
	4	61,819.779	3.1	64,906.29	1.7	61,819.779	3.1	64,906.29	1.7
	5	63,186.758	2.3	64,989.994	1.6	63,186.758	2.3	64,989.994	1.6
	1	67,067.547	24.3	67,067.547	27.9	67,067.547	27.5	67,067.547	31.2
	2	68,045.156	18.2	0.0	23.4	68,045.156	19.3	0.0	24.3
55	3	76,196.767	2.2	76,196.767	1.8	76,196.767	2.2	76,196.767	1.8
	4	77,185.041	1.8	78,403.061	1.7	77,185.041	1.8	78,403.061	1.6
	5	77,269.145	1.8	78,119.798	1.6	77,269.145	1.7	78,119.798	1.5
	1	0.0	56.8	0.0	68.1	0.0	62.1	0.0	72.8

(continued on next page)

**Table 2** (continued)

$A^+ + K \rightarrow A(k) + K^+$									
40 keV									
$A^+$	Initial (0.0 cm)			Final (120.0 cm)			5 keV		
(Z)	#	Level (cm <sup>-1</sup> )	%	Level (cm <sup>-1</sup> )	%	Level (cm <sup>-1</sup> )	%	Level (cm <sup>-1</sup> )	%
56	2	11,178.26816	3.3	18,535.5286	0.9	11,178.26816	2.9	18,535.5286	0.8
	3	11,732.3071	2.9	22,588.821	0.5	11,732.3071	2.6	22,588.821	0.4
	4	14,499.2568	1.7	22,631.6863	0.5	14,499.2568	1.6	22,631.6863	0.4
	5	14,596.84232	1.7	24,317.1494	0.4	14,596.84232	1.5	24,317.1494	0.3
	1	0.0	48.8	0.0	27	0.0	98.3	0.0	95.5
57 <sup>†</sup>	2	9033.966	9.1	9033.966	15.7	9033.966	0.4	9033.966	1.2
	3	9215.501	8.6	9215.501	14.8	9215.501	0.3	9215.501	1.1
	4	9596.533	7.7	9596.533	12.8	9596.533	0.3	9596.533	0.9
	5	11,395.35	4.5	12,266.024	5.8	11,395.35	0.1	12,266.024	0.3
	1	3494.526	7.2			3494.526	22.8		
58 <sup>†</sup>	2	4121.572	7.1			3010.002	20.7		
	3	3010.002	7.1			4121.572	20.4		
	4	2668.188	6.9			2668.188	17.8		
	5	1053.164	5.7			1053.164	5.3		
	1	3312.24	1.2			3210.583	4.2		
59 <sup>†</sup>	2	3210.583	1.2			3196.607	4.2		
	3	3196.607	1.2			3312.24	4.1		
	4	3100.151	1.2			3100.151	4.1		
	5	3710.513	1.2			3710.513	3.9		
	1	2846.75	3.6			2846.75	25.3		
60	2	1376.6	3.3			1376.6	14.9		
	3	4381.1	3.3			4381.1	11.5		
	4	4432.22	3.3			4432.22	11.0		
	5	4866.54	3.1			4866.54	7.6		
	1	3681.696	3.8	3681.696	3.3	3681.696	28.7	3681.696	28
61 <sup>†</sup>	2	2366.597	3.7	2366.597	3.2	2366.597	26.3	2366.597	25.6
	3	5048.602	3.4	5048.602	2.9	5048.602	11.5	5048.602	11.2
	4	1128.056	3.3	1128.056	2.8	1128.056	10.9	1128.056	10.6
	5	0.0	2.7	0.0	2.5	0.0	4.2	0.0	4.1
	1	3919.03	9			3919.03	22.6		
62	2	2797.1	8.7			2797.1	19.1		
	3	5089.79	8.4			5089.79	11.9		
	4	5249.48	8.3			5249.48	10.5		
	5	5460.5	8.1			1748.78	9.2		
	1	4020.66	7.1	4020.66	7.1	4020.66	37.9	4020.66	37.8
63	2	3125.46	6.8	3125.46	6.7	3125.46	27.7	3125.46	27.6
	3	2273.09	6.1	2273.09	6.1	2273.09	14.5	2273.09	14.5
	4	1489.55	5.4	1489.55	5.4	1489.55	7.2	1489.55	7.2
	5	811.92	4.7	811.92	4.7	811.92	3.9	811.92	3.9
	1	0.0	19.1	0.0	46.4	0.0	60.7	0.0	82.2
64	2	12,923.72	5.6	15,137.72	4.7	12,923.72	3.4	15,137.72	1.7
	3	13,048.9	5.4	15,248.76	4.6	13,048.9	3.2	15,248.76	1.7
	4	13,222.04	5.1	15,421.25	4.5	13,222.04	2.9	15,421.25	1.6
	5	13,457.21	4.8	15,680.28	4	13,457.21	2.7	15,680.28	1.4
	1	8498.434	2.8	10,222.233	4	7947.294	9.3	7653.927	13.8
65 <sup>†</sup>	2	7947.294	2.8	10,359.905	3.9	8498.434	9.1	7562.457	13.3
	3	7653.927	2.8	10,576.41	3.8	7653.927	8.6	7426.71	12.5
	4	7562.457	2.8	10,883.505	3.6	7562.457	8.3	7234.91	11.2
	5	7480.348	2.8	7653.927	3.6	7480.348	8.0	6976.508	9.4
	1	5829.86	2.2			5829.86	6.0		
66	2	6259.09	2.1			5483.98	5.7		
	3	6351.75	2.1			6259.09	5.6		
	4	6488.28	2.1			5425.06	5.6		
	5	5483.98	2.1			6351.75	5.5		
	1	7050.603	8.5	7050.603	9.3	7050.603	35.2	7050.603	35.5
67	2	7565.61	8.2	7565.61	9	7565.61	25.9	7565.61	26.2
	3	8519.21	7.3	8519.21	8.1	8519.21	11.5	8519.21	11.6
	4	4134.222	6.7	4134.222	7.8	4134.222	9.1	4134.222	9.2
	5	9211.591	6.5	9211.591	7.1	9211.591	6.0	9211.591	6
	1	8605.16	22.6	8605.16	24.5	8605.16	49.2	8605.16	49.6
68	2	5419.7	21.3	5419.7	23	5419.7	40.5	5419.7	40.8
	3	10,695.75	15.2	10,695.75	16.5	10,695.75	7.0	10,695.75	7
	4	13,094.42	7.5	0.0	6.7	13,094.42	1.1	0.0	0.7
	5	0.0	5.3	13,094.42	4.4	0.0	0.6	13,094.42	0.6
	1	6958.329	18.7	6958.329	20.9	6958.329	69.7	6958.329	74.3
69	2	10,750.982	14	10,750.982	15.6	5035.193	13.0	10,750.982	11.6
	3	5035.193	13.9	5035.193	9.8	10,750.982	10.9	5035.193	8.8
	4	12,377.534	9.2	12,377.534	6.5	12,377.534	2.5	12,377.534	1.7
	5	13,097.906	7.4	13,097.906	5.2	13,097.906	1.4	13,097.906	1

(continued on next page)

**Table 2** (continued)

$A^+ + K \rightarrow A(k) + K^+$									
40 keV									
A <sup>+</sup>	Initial (0.0 cm)				5 keV				
	(Z)	#	Level (cm <sup>-1</sup> )	%	Level (cm <sup>-1</sup> )	%	Level (cm <sup>-1</sup> )	%	
69	1	8771.243	63.7	8771.243	60.7	8771.243	99.1	8771.243	99
	2	0.0	8.9	0.0	10.5	0.0	0.3	0.0	0.3
	3	20,406.84	2.5	22,419.764	2.2	20,406.84	0.1	22,419.764	0
	4	21,799.38	1.6	22,559.502	2.1	21,799.38	0.0	22,559.502	0
	5	22,419.764	1.3	20,406.84	2.1	22,419.764	0.0	20,406.84	0
70	1	17,288.439	26.7	0.0	36.3	17,288.439	28.6	0.0	37.3
	2	0.0	23.2	17,288.439	33	0.0	25.5	17,288.439	35.8
	3	17,992.007	20.9	19,710.388	14.2	17,992.007	20.6	19,710.388	12.9
	4	19,710.388	11.5	24,489.102	3.2	19,710.388	10.3	24,489.102	2.9
	5	24,489.102	2.6	24,751.948	3	24,489.102	2.3	24,751.948	2.7
71	1	1993.92	31.1	1993.92	31.6	1993.92	63.4	1993.92	63.4
	2	4136.13	27.5	4136.13	27.6	4136.13	21.9	4136.13	21.9
	3	0.0	24.2	0.0	25.7	0.0	13.6	0.0	13.6
	4	7476.39	11.7	7476.39	11.7	7476.39	1.0	7476.39	1
	5	17,427.28	0.4	18,851.31	0.3	17,427.28	0.0	18,851.31	0
72	1	14,017.83	6.9	14,092.28	9.3	14,017.83	19.6	14,092.28	22.9
	2	14,092.28	6.9	14,740.68	8.9	14,092.28	19.1	14,017.83	17.7
	3	14,435.13	6.8	15,673.33	7.8	14,435.13	15.9	14,740.68	15.3
	4	14,541.68	6.7	14,017.83	7	14,541.68	14.8	14,435.13	14.3
	5	14,740.68	6.6	14,435.13	6.8	14,740.68	12.7	14,541.68	13.3
73	1	19,657.78	2.7	0.0	6.3	19,657.78	10.2	0.0	12.8
	2	19,178.45	2.7	20,646.54	3.7	19,178.45	10.1	19,657.78	12.1
	3	20,340.39	2.6	21,153.33	3.5	20,340.39	7.5	20,646.54	9.9
	4	20,560.26	2.6	21,622.92	3.2	18,504.72	7.2	19,178.45	8.4
	5	18,504.72	2.5	23,355.41	3.2	20,560.26	6.4	21,153.33	6.2
74	1	22,476.68	2.6	2951.29	8.9	22,476.68	8.5	1670.29	19.4
	2	21,453.9	2.6	1670.29	8.6	21,453.9	8.4	0.0	10.2
	3	21,448.76	2.6	0.0	6.4	21,448.76	8.3	22,476.68	9.4
	4	22,773.78	2.6	4830.0	4.8	22,773.78	7.3	23,047.31	9.3
	5	22,852.8	2.6	23,047.31	4.3	22,852.8	6.9	22,773.78	8.1
75 <sup>†</sup>	1	21,775.4	4.9			21,775.4	17.0		
	2	22,160.04	4.9			22,160.04	15.7		
	3	22,422.83	4.8			22,422.83	13.9		
	4	23,154.81	4.5			20,481.73	9.0		
	5	20,481.73	4.5			20,447.8	8.8		
76 <sup>†</sup>	1	25,601.55	3.8			25,601.55	10.8		
	2	25,593.94	3.8			25,593.94	10.7		
	3	27,954.32	3.8			27,954.32	8.2		
	4	28,139.52	3.7			25,275.42	8.1		
	5	25,275.42	3.7			28,139.52	6.8		
77	1	30,529.66	6	0.0	27.7	30,529.66	32.3	30,529.66	29.7
	2	32,463.58	5.5	7106.61	8.5	32,463.58	13.0	7106.61	16.1
	3	32,513.43	5.4	5784.62	8.2	32,513.43	12.4	0.0	15.5
	4	32,830.78	5.1	32,830.78	7	32,830.78	8.9	5784.62	12.4
	5	33,064.83	4.9	2834.98	6.5	33,064.83	7.0	32,830.78	11.5
78 <sup>†</sup>	1	30,157.0	31.3			30,157.0	93.2		
	2	26,638.6	14.9			26,638.6	3.4		
	3	36,296.4	10			36,296.4	1.1		
	4	36,781.6	8.5			36,781.6	0.7		
	5	38,536.2	4.6			38,536.2	0.3		
79	1	37,358.991	51.5	0.0	65.4	37,358.991	80.6	0.0	87.3
	2	41,174.613	13.8	42,163.53	9.8	41,174.613	6.6	42,163.53	4.1
	3	42,163.53	9.8	21,435.191	5.5	42,163.53	4.1	21,435.191	2.2
	4	21,435.191	5.5	45,537.195	3.3	21,435.191	2.2	45,537.195	1.1
	5	45,537.195	3.3	46,174.979	2.7	45,537.195	1.1	46,174.979	0.9
80	1	44,042.909	47.6	44,042.909	48.7	44,042.909	85.9	44,042.909	86
	2	39,412.237	29.9	0.0	31.4	39,412.237	11.3	0.0	11.4
	3	37,644.982	17.6	37,644.982	18.5	37,644.982	2.6	37,644.982	2.6
	4	54,068.6829	2.1	71,336.005	0	54,068.6829	0.1	71,336.005	0
	5	62,350.325	0.2	70,932.2	0	62,350.325	0.0	76,466.936	0
81	1	7792.7	86.3	7792.7	86.4	7792.7	99.7	7792.7	99.7
	2	0.0	12	0.0	12.6	0.0	0.3	0.0	0.3
	3	26,477.5	0.5	34,159.9	0.1	26,477.5	0.0	34,159.9	0
	4	34,159.9	0.1	35,161.1	0.1	34,159.9	0.0	35,161.1	0
	5	35,161.1	0.1	41,368.1	0	35,161.1	0.0	46,949.9	0
82	1	45,443.171	6.2	10,650.3271	11.4	45,443.171	5.9	10,650.3271	10.6
	2	46,060.8364	5.6	7819.2626	5.7	46,060.8364	5.3	7819.2626	5.6
	3	46,068.4385	5.6	0.0	5.6	46,068.4385	5.3	0.0	5.3
	4	46,328.6668	5.3	52,101.66	2.1	46,328.6668	5.1	52,101.66	2.1

(continued on next page)

**Table 2** (continued)

$A^+ + K \rightarrow A(k) + K^+$									
40 keV									
$A^+$		Initial (0.0 cm)		Final (120.0 cm)		5 keV			
(Z)	#	Level ( $\text{cm}^{-1}$ )	%						
83	5	52,101.66	2.1	52,311.315	2.1	52,101.66	2.1	52,311.315	2.1
	1	15,437.501	52.6	15,437.501	52.9	15,437.501	90.2	15,437.501	90.2
	2	21,660.914	28	21,660.914	28.1	21,660.914	7.2	21,660.914	7.2
	3	11,419.039	16.4	11,419.039	16.6	11,419.039	2.5	11,419.039	2.5
	4	32,588.221	0.8	0.0	0.9	32,588.221	0.0	0.0	0.1
84 <sup>†</sup>	5	0.0	0.7	33,164.805	0.7	0.0	0.0	33,164.805	0
	1	21,679.11	70.9			21,679.11	89.9		
	2	16,831.61	14.8			16,831.61	5.8		
	3	39,081.19	4.9			39,081.19	1.5		
	4	40,802.7	3			40,802.7	0.9		
85 <sup>‡</sup>	5	42,718.0	1.8			42,718.0	0.5		
	1	54,620.35	45.5			54,620.35	49.2		
	2	55,989.03	28			55,989.03	27.6		
	3	66,244.97	1.8			66,244.97	1.6		
	4	66,707.53	1.6			66,707.53	1.4		
86 <sup>†</sup>	5	67,906.52	1.3			67,906.52	1.1		
	1	0.0	78.4	0.0	88.7	0.0	83.1	0.0	91.7
	2	12,237.409	2.4	16,229.87	1.4	12,237.409	1.9	16,229.87	1.2
	3	13,923.998	1.7	16,429.64	1.3	13,923.998	1.3	16,429.64	1.1
	4	16,229.87	1.1	19,739.98	0.9	16,229.87	0.9	19,739.98	0.9
87 <sup>†</sup>	5	16,429.64	1.1	30,936.325	0.1	16,429.64	0.8	30,936.325	0.1
	1	2231.43	43.2			2231.43	80.4		
	2	0.0	34			0.0	18.8		
	3	9217.28	5.5			9217.28	0.2		
	4	9863.59	4.3			9863.59	0.1		
88 <sup>‡</sup>	5	10,000.0	4			10,000.0	0.1		

elements are usually inaccessible to laser spectroscopy due to the vacuum-UV lasers that would be required for transitions from their atomic ground states. The high reactivity of the elements also poses its own experimental challenges, molecular formation is highly probable with the traps often used for high-resolution laser spectroscopy. Laser spectroscopy studies of these elements would be important for both nuclear structure [62] and environmental sciences [63,64,65]. Measurements of these light elements are planned for the near future at the CRIS experiment [66].

While the calculations were performed for  $1 \leq Z \leq 89$  for completeness, the reliability is unknown for very light or heavy systems or for systems for which little atomic data is known, as no experimental data is available for comparison. These particular cases are indicated in Tables 2 and 3. For elements with  $1 \leq Z \leq 3$  at a beam energy of  $T_B = 40 \text{ keV}$ , their velocities are already above the limit of the assumed intermediate velocity region. The validity of the above approach diminishes for heavier masses, where relativistic calculations are needed [67]. For lighter masses such as hydrogen or helium, much experimental data as well as advanced cross-section calculations are already widely available however [41]. For many elements there exists limited experimental atomic transition probability data, and in some cases even atomic level data is limited. For these systems only the initial populations prior to the decay part of the simulations are included in the tables, although their atomic analogues can be used as a guide.

The total cross-sections used to normalize the relative populations in this work are given in Table 4. Although accuracy of the values depends highly on the completeness of atomic data, the values can be used for estimations, and to determine the cross-section for the direct population of the states listed in Tables 2 and 3.

#### 4.2. High-lying state population background

Due to the high level density near the atomic continuum and the

long life times of high-lying Rydberg states, even for small cross sections for populating these states their sum contribution can be large, which constitutes a large relative atomic population near the IP of the atom. The population of these high lying states creates a fraction of the atomic ensemble which have a higher probability for laser-induced and collisional ionization [15], significantly contributing to background of CLS experiments. Using the relative atomic population results already discussed, the fraction of the atomic population within the reach of Nd:YAG laser harmonic wavelengths is shown in Fig. 5. These are typical non-resonant laser ionization pulse wavelengths used for CRIS. The values give a measure of the background one can expect for each element. The population of these states is highest for elements with a difference in IP from potassium or sodium close to its own IP i.e.  $I_B \approx 2I_A$ . In these cases the population of the high-lying states will be proportional to the total cross section for neutralisation, and the energy dependence can be seen in Table 9. At online isotope separation facilities such as ISOLDE, isobaric contamination can be many orders of magnitude larger than the isotope of interest [68]. Therefore knowledge of the magnitude of this source of background for each element is important. Experimentally, this source of background can be reduced with the use of field-ionization plates [69], or non-resonant ionization laser pulses before the measurement window, for bunched beam CLS experiments.

#### 4.3. Asymmetric lineshapes

For the measurements of the hyperfine structure of  $^{113,115}\text{In}$ , peak asymmetry was observed in the spectra of both the  $5\text{p } ^2\text{P}_{3/2} \rightarrow 9\text{s } ^2\text{S}_{1/2}$  (246.8 nm) and  $5\text{p } ^2\text{P}_{1/2} \rightarrow 8\text{s } ^2\text{S}_{1/2}$  (246.0 nm) transitions, which from simulation was expected to be due to the population of the  $5\text{p } ^2\text{P}_{1/2}$  and  $5\text{p } ^2\text{P}_{3/2}$  states by intermediate states following neutralisation (as shown in Fig. 6).

The additional energy defect  $E^*$  required to populate these states

**Table 3**

Atomic population distribution simulation results for neutralisation of an ion beam of elements A = 1–90 by free Na atoms. Atomic data sourced from the NIST atomic database[48]. Only the 5 most populous states are listed in this table. † - insufficient transition data was available for these elements. \* - these light elements are outside of the intermediate velocity region at 40 keV. The columns for 0 cm and 120 cm flight distance give respectively the initial populations after charge exchange at 0 cm and the final populations after a further 120 cm of atom flight at the corresponding beam energy.

$A^+ + K \rightarrow A(k) + K^+$								
40 keV								
$A^+$		Initial (0.0 cm)		Final (120.0 cm)		5 keV		
(Z)	#	Level ( $\text{cm}^{-1}$ )	%	Level ( $\text{cm}^{-1}$ )	%	Level ( $\text{cm}^{-1}$ )	%	Level ( $\text{cm}^{-1}$ )
1*	1	107,965.04916	1	0.0	41.5	82,258.91911	4.4	0.0
	2	107,965.04971	1	82,258.9544	1.8	82,258.9544	4.4	82,258.9544
	3	107,965.05487	1	107,440.43933	1	82,259.158	4.4	107,440.4385
	4	107,965.05488	1	108,324.72418	1	82,259.285	4.4	107,440.43933
	5	107,965.05677	1	108,324.72416	1	97,492.2112	1.8	107,965.04916
2*	1	166,277.44014	1.2	159,855.97433	52.9	159,855.97433	16.4	159,855.97433
	2	169,086.76647	1.2	0.0	9.1	166,277.44014	10.4	0.0
	3	169,086.8429	1.2	193,921.61495	0.7	169,086.76647	7.5	166,277.44014
	4	169,087.83081	1.2	193,921.61772	0.7	169,086.8429	7.5	193,921.61495
	5	159,855.97433	1.2	193,921.62024	0.7	169,087.83081	7.5	193,921.61772
3*	1	0.0	4.4	0.0	52.5	0.0	53.2	0.0
	2	14,903.66	4.1	42,003.3	0.7	14,903.66	12.5	42,003.3
	3	14,904.0	4.1	42,298.0	0.7	14,904.0	12.5	42,298.0
	4	27,206.12	2.4	42,389.0	0.7	27,206.12	1.4	42,389.0
	5	30,925.38	1.8	42,389.0	0.7	30,925.38	0.7	42,389.0
4	1	42,565.35	4.2	21,978.28	64.2	42,565.35	26.8	21,978.28
	2	21,981.27	3.1	21,978.925	15.5	21,981.27	15.0	21,978.925
	3	21,978.925	3.1	0.0	6.3	21,978.925	15.0	21,981.27
	4	21,978.28	3.1	21,981.27	5.9	21,978.28	15.0	0.0
	5	52,080.94	2.9	56,882.43	1.6	52,080.94	3.3	56,882.43
5	1	28,647.43	7	0.0	37.1	28,647.43	30.6	28,647.43
	2	28,652.07	7	15.287	14.4	28,652.07	30.6	28,652.07
	3	28,658.4	7	28,647.43	6.9	28,658.4	30.5	28,658.4
	4	40,039.6907	5.2	28,652.07	6.9	40,039.6907	2.6	0.0
	5	47,856.809	3.2	28,658.4	6.9	15.287	0.5	15.287
6	1	60,333.43	2.2	16.4	36.7	60,333.43	11.7	16.4
	2	60,352.63	2.1	0.0	21.1	60,352.63	11.7	0.0
	3	60,393.14	2.1	43.4	13.4	60,393.14	11.6	43.4
	4	61,981.82	2	10,192.63	6	61,981.82	7.9	10,192.63
	5	64,086.92	1.8	33,735.2	0.8	33,735.2	4.9	33,735.2
7	1	83,284.07	2.4	0.0	54.7	83,284.07	16.2	0.0
	2	83,317.83	2.4	19,224.464	8	83,317.83	16.0	19,224.464
	3	83,364.62	2.4	19,233.177	5.1	83,364.62	15.8	19,233.177
	4	86,137.35	2.2	28,838.92	1.1	86,137.35	7.5	28,838.92
	5	86,220.51	2.2	106,868.635	1	86,220.51	7.3	106,868.635
8	1	73,768.2	6.1	73,768.2	46.8	73,768.2	54.6	73,768.2
	2	76,794.978	5.5	0.0	19.9	76,794.978	23.1	0.0
	3	86,625.757	2.7	158.265	4.1	86,625.757	1.5	158.265
	4	86,627.778	2.7	102,865.655	0.9	86,627.778	1.5	102,865.655
	5	86,631.454	2.7	226.977	0.7	86,631.454	1.5	105,441.645
9	1	102,405.71	6	102,405.71	19.1	102,405.71	23.4	102,405.71
	2	102,680.44	6	102,680.44	16	102,680.44	22.0	102,680.44
	3	102,840.38	6	102,840.38	10.8	102,840.38	21.2	102,840.38
	4	104,731.05	5.7	104,731.05	7.8	104,731.05	12.8	104,731.05
	5	105,056.28	5.6	105,056.28	5.1	105,056.28	11.7	105,056.28
10	1	134,041.84	6.6	0.0	25.2	134,041.84	26.4	0.0
	2	134,459.2871	6.6	134,041.84	22.1	134,459.2871	24.9	134,041.84
	3	134,818.6405	6.6	134,818.6405	7.1	134,818.6405	23.5	134,818.6405
	4	135,888.7173	6.5	158,601.1152	2	135,888.7173	18.9	158,601.1152
	5	148,257.7898	2.7	159,379.9935	0.8	148,257.7898	0.5	159,379.9935
11	1	0.0	26.4	0.0	72.9	0.0	95.5	0.0
	2	16,956.17025	8.4	37,059.54	0.5	16,956.17025	0.8	37,059.54
	3	16,973.36619	8.4	38,400.9	0.4	16,973.36619	0.8	38,400.9
	4	25,739.999	2.5	38,400.904	0.4	25,739.999	0.1	38,400.904
	5	29,172.837	1.5	38,401.147	0.4	29,172.837	0.1	38,401.147
12	1	21,850.405	13.4	21,870.464	27.8	21,850.405	32.6	21,850.405
	2	21,870.464	13.4	21,850.405	26	21,870.464	32.5	21,870.464
	3	21,911.178	13.4	21,911.178	22	21,911.178	32.3	21,911.178
	4	35,051.264	5.3	0.0	6.3	35,051.264	0.5	0.0
	5	0.0	2.9	46,403.065	2.3	0.0	0.2	46,403.065
13	1	112.061	18.4	0.0	41.5	112.061	46.9	0.0
	2	0.0	18.3	112.061	30.3	0.0	45.1	112.061
	3	25,347.756	5.8	29,020.41	3.5	25,347.756	1.2	29,020.41
	4	29,020.41	3.5	29,066.96	3.5	29,020.41	0.6	29,066.96
	5	29,066.96	3.5	29,142.78	3.4	29,066.96	0.5	29,142.78

(continued on next page)

**Table 3** (continued)

$A^+ + K \rightarrow A(k) + K^+$									
40 keV									
$A^+$		Initial (0.0 cm)		Final (120.0 cm)		5 keV			
(Z)	#	Level (cm <sup>-1</sup> )	%						
14	1	33,326.053	8.5	77.115	27.9	15,394.37	32.8	33,326.053	25
	2	15,394.37	7.6	0.0	22.6	33,326.053	27.6	77.115	24.4
	3	39,683.163	4.2	223.157	8.3	39,683.163	3.5	0.0	18.3
	4	39,760.285	4.2	6298.85	5.3	39,760.285	3.4	15,394.37	7.6
	5	39,955.053	4	33,326.053	5.2	39,955.053	3.2	223.157	5.7
15	1	55,939.421	4.2	0.0	30	55,939.421	9.9	0.0	50.6
	2	56,090.626	4.1	11,361.02	6.5	56,090.626	9.5	11,361.02	8.4
	3	56,339.656	4	65,788.455	1.9	56,339.656	8.7	65,788.455	1.4
	4	57,876.574	3.3	65,585.13	1.9	57,876.574	5.5	65,585.13	1.4
	5	58,174.366	3.2	65,450.125	1.9	58,174.366	5.1	65,450.125	1.4
16	1	52,623.64	10.8	0.0	38.5	52,623.64	36.5	0.0	47.6
	2	55,330.811	7.8	52,623.64	32.1	55,330.811	14.9	52,623.64	31.7
	3	22,179.954	3.5	63,446.065	13.6	22,179.954	4.3	63,446.065	8
	4	63,446.065	2.6	396.055	6.9	63,446.065	1.9	396.055	8
	5	63,457.142	2.6	573.64	2.6	63,457.142	1.9	573.64	1.3
17	1	71,958.363	7.7	0.0	42.4	71,958.363	22.5	0.0	67.2
	2	72,488.568	7.3	71,958.363	12.2	72,488.568	18.3	882.3515	17.1
	3	72,827.038	7	882.3515	12.1	72,827.038	16.1	71,958.363	6.1
	4	74,225.846	5.9	87,979.49	1.1	74,225.846	9.7	87,979.49	0.4
	5	74,865.667	5.4	88,080.042	1.1	74,865.667	7.8	88,080.042	0.4
18	1	93,143.76	11.3	0.0	29.3	93,143.76	30.0	93,143.76	40.8
	2	93,750.5978	10.5	93,143.76	28.6	93,750.5978	22.9	0.0	36.6
	3	94,553.6652	9.5	94,553.6652	9.6	94,553.6652	16.1	94,553.6652	12.8
	4	95,399.8276	8.5	112,750.153	1.1	95,399.8276	11.4	112,750.153	0.3
	5	104,102.099	2.1	113,716.555	0.9	104,102.099	0.8	113,716.555	0.3
19	1	0.0	36.5	0.0	65.5	0.0	87.8	0.0	94
	2	12,985.18572	5.4	30,617.31	0.4	12,985.18572	1.2	30,617.31	0.1
	3	13,042.89603	5.4	30,617.31	0.4	13,042.89603	1.1	30,617.31	0.1
	4	21,026.551	1.5	33,910.42	0.3	21,026.551	0.3	33,910.42	0
	5	21,534.68	1.4	33,910.42	0.3	21,534.68	0.3	33,910.42	0
20	1	15,157.901	10.3	15,210.063	14.9	15,157.901	21.2	15,157.901	25.8
	2	15,210.063	10.2	15,157.901	14.4	15,210.063	20.7	15,210.063	24.8
	3	15,315.943	10.1	15,315.943	14	15,315.943	19.7	15,315.943	23.9
	4	0.0	8.7	20,335.36	9.3	0.0	18.7	0.0	8.5
	5	20,335.36	5.1	20,349.26	8.3	20,335.36	2.7	20,335.36	4
21	1	11,677.38	3.3	0.0	12.3	11,519.99	11.8	11,519.99	13.9
	2	11,610.28	3.3	168.34	10.6	11,557.69	11.8	11,557.69	13.9
	3	11,557.69	3.3	11,519.99	6.2	11,610.28	11.8	11,610.28	13.9
	4	11,519.99	3.3	11,557.69	5.7	11,677.38	11.8	11,677.38	13.9
	5	14,926.07	3	11,610.28	5.6	14,926.07	4.6	0.0	8.5
22	1	14,105.634	1.4	0.0	6	13,981.773	5.3	15,877.081	5.4
	2	14,028.436	1.4	386.874	5.2	14,028.436	5.3	16,106.076	4.9
	3	13,981.773	1.4	170.1328	4.9	14,105.634	5.2	15,975.631	4.7
	4	15,108.111	1.4	6598.765	4.3	15,108.111	4.3	15,108.111	4.2
	5	15,156.802	1.4	6742.756	3.8	15,156.802	4.3	15,156.802	4.2
23	1	13,801.54	1.3	2153.21	6.2	13,801.54	4.7	14,909.97	4.1
	2	13,810.94	1.3	2220.11	5.6	13,810.94	4.7	14,949.37	4
	3	14,514.76	1.3	2311.36	4.9	14,514.76	3.9	15,000.94	3.9
	4	14,548.81	1.3	2112.28	4.3	14,548.81	3.9	15,062.96	3.9
	5	14,909.97	1.3	2424.78	4.2	11,100.59	3.4	2220.11	3.4
24	1	8307.5753	2.8	0.0	11.5	8307.5753	11.1	8307.5753	11.4
	2	8095.1842	2.8	7593.1484	6.6	8095.1842	10.0	8095.1842	10.4
	3	7927.441	2.7	7810.7795	4.2	7927.441	9.2	7927.441	9.6
	4	7810.7795	2.7	7927.441	4.2	7810.7795	8.7	7593.1484	9.4
	5	7750.7465	2.7	8095.1842	4.1	7750.7465	8.5	7810.7795	9.1
25	1	18,705.37	4.3	0.0	13.6	18,531.64	11.9	18,705.37	14.6
	2	18,531.64	4.3	18,402.46	6.8	18,705.37	11.8	18,402.46	13.8
	3	18,402.46	4.3	18,705.37	6.6	18,402.46	11.8	18,531.64	13.5
	4	17,637.15	4.2	18,531.64	6.4	17,637.15	10.7	17,637.15	9.9
	5	17,568.48	4.2	17,451.52	5.6	17,568.48	10.5	17,568.48	9.8
26	1	22,650.416	1.3	0.0	8	22,249.429	3.2	22,650.416	5.4
	2	22,838.323	1.3	415.933	6.2	22,650.416	3.2	23,270.384	5
	3	22,845.869	1.3	704.007	5.8	21,999.13	3.2	0.0	4.4
	4	22,946.816	1.3	888.132	4.7	22,838.323	3.1	23,244.838	4.3
	5	22,996.674	1.3	19,350.891	2.4	22,845.869	3.1	23,192.5	4.1
27	1	22,475.36	2	0.0	7.7	21,920.09	6.4	23,611.78	9.1
	2	23,152.57	2	816.0	5.9	22,475.36	6.4	23,855.62	8.3
	3	21,920.09	2	1406.84	4.7	21,780.47	6.4	24,326.11	6.8
	4	23,184.23	2	1809.33	3.6	21,215.9	5.8	24,733.28	5.6

(continued on next page)

**Table 3** (continued)

$A^+ + K \rightarrow A(k) + K^+$									
40 keV									
$A^+$		Initial (0.0 cm)		Final (120.0 cm)		5 keV			
(Z)	#	Level (cm <sup>-1</sup> )	%						
28	5	23,207.76	2	23,611.78	3.6	23,152.57	5.7	25,041.16	4.7
	1	22,102.325	4.5	204.787	16	22,102.325	32.6	22,102.325	16.5
	2	16,017.306	3.5	0.0	13.7	16,017.306	10.3	0.0	11.5
	3	15,734.001	3.4	879.816	12.1	15,734.001	8.8	16,017.306	9.3
	4	15,609.844	3.4	1713.087	6.6	15,609.844	8.2	25,753.553	9
29	5	25,753.553	3.3	1332.164	5	14,728.84	5.1	204.787	8.7
	1	13,245.443	18.8	0.0	39.9	13,245.443	41.7	13,245.443	41.8
	2	30,535.324	14	13,245.443	19.2	11,202.618	17.8	0.0	31.7
	3	11,202.618	13.5	11,202.618	16.7	30,535.324	14.3	11,202.618	18.9
	4	30,783.697	13.4	39,018.69	2.7	30,783.697	12.9	39,018.69	1
30	5	39,018.69	2.7	40,909.16	1.9	39,018.69	1.0	40,909.16	0.7
	1	32,890.352	27.1	32,890.352	29.4	32,890.352	37.8	32,890.352	37.9
	2	32,501.421	26.4	32,501.421	28.7	32,501.421	32.2	32,501.421	32.3
	3	32,311.35	26.1	32,311.35	28.4	32,311.35	29.5	32,311.35	29.6
	4	46,745.413	5.5	46,745.413	2	46,745.413	0.2	46,745.413	0.1
31	5	53,672.28	1.4	53,672.28	1.5	53,672.28	0.0	53,672.28	0
	1	826.19	39.7	826.19	41.6	826.19	58.0	826.19	58.2
	2	0.0	34.7	0.0	40.2	0.0	37.8	0.0	38.8
	3	24,788.53	3.9	33,044.05	0.8	24,788.53	0.7	33,044.05	0.1
	4	33,044.05	0.8	33,155.07	0.8	33,044.05	0.1	33,155.07	0.1
32	5	33,155.07	0.8	37,975.768	0.4	33,155.07	0.1	37,975.768	0.1
	1	16,367.3332	39.9	557.1341	28.3	16,367.3332	83.5	16,367.3332	42.6
	2	7125.2989	7.3	0.0	18.6	7125.2989	2.4	557.1341	17.8
	3	37,451.6893	6	16,367.3332	8.8	37,451.6893	1.7	0.0	12
	4	37,702.3054	5.7	1409.9609	7.5	37,702.3054	1.6	1409.9609	4.6
33	5	39,117.9021	4.1	7125.2989	4.9	39,117.9021	1.1	7125.2989	3.7
	1	50,693.8	12.2	50,693.8	16.1	50,693.8	14.1	50,693.8	18.4
	2	51,610.2	9.8	51,610.2	13	51,610.2	10.7	51,610.2	13.9
	3	52,897.9	7.3	52,897.9	9.6	52,897.9	7.4	52,897.9	9.7
	4	53,135.6	6.9	55,366.4	5.5	53,135.6	7.0	55,366.4	5.2
34 <sup>†</sup>	5	54,605.3	4.9	53,135.6	4.6	18,647.5	5.0	53,135.6	4.6
	1	48,182.19	24.1			48,182.19	33.4		
	2	50,996.931	12.2			22,446.202	13.7		
	3	22,446.202	11.9			50,996.931	12.6		
	4	59,242.798	1.9			59,242.798	1.6		
35	5	59,287.818	1.9			59,287.818	1.5		
	1	63,436.45	19.7	63,436.45	23.8	63,436.45	30.6	63,436.45	35.4
	2	64,907.19	13.9	64,907.19	16.8	64,907.19	17.0	64,907.19	19.7
	3	66,883.87	8.6	66,883.87	10.4	66,883.87	8.5	66,883.87	9.8
	4	67,183.58	8	67,183.58	4.8	67,183.58	7.7	67,183.58	4.4
36	5	68,970.21	5.2	68,970.21	3.1	68,970.21	4.4	68,970.21	2.6
	1	79,971.7417	23.5	79,971.7417	30.2	79,971.7417	36.6	79,971.7417	42.6
	2	80,916.768	18.8	80,916.768	22.6	80,916.768	23.7	80,916.768	26.3
	3	85,191.6166	6.6	85,191.6166	5.5	85,191.6166	5.1	85,191.6166	4.1
	4	85,846.7046	5.6	85,846.7046	5.1	85,846.7046	4.3	85,846.7046	3.6
37	5	91,168.515	1.6	91,168.515	1.5	91,168.515	1.2	91,168.515	1
	1	0.0	58.5	0.0	63.3	0.0	79.6	0.0	82.3
	2	12,578.95	3	12,816.545	3.2	12,578.95	1.6	12,816.545	1.6
	3	12,816.545	2.9	19,355.203	0.9	12,816.545	1.5	19,355.203	0.5
	4	19,355.203	0.9	19,355.649	0.9	19,355.203	0.5	19,355.649	0.5
38	5	19,355.649	0.9	20,132.51	0.8	19,355.649	0.5	20,132.51	0.4
	1	0.0	33.9	0.0	20.1	0.0	82.4	0.0	66.7
	2	14,317.507	11.6	14,317.507	17.3	14,317.507	3.9	14,317.507	9.3
	3	14,504.334	11.1	14,898.545	14.4	14,504.334	3.6	14,898.545	7.1
	4	14,898.545	10.1	14,504.334	13.5	14,898.545	3.1	14,504.334	4.9
39	5	18,159.04	4.5	18,159.04	7.8	18,159.04	1.0	18,159.04	2.9
	1	10,529.169	6.1	0.0	6.7	10,529.169	20.5	10,529.169	20.5
	2	10,937.39	5.9	10,937.39	6.2	10,937.39	15.9	10,937.39	16
	3	11,078.614	5.8	10,529.169	6.1	11,078.614	14.5	11,078.614	14.5
	4	11,277.928	5.7	11,078.614	5.9	11,277.928	12.7	11,277.928	12.7
40 <sup>†</sup>	5	11,359.757	5.6	11,277.928	5.9	11,359.757	12.0	11,359.757	12
	1	12,342.37	2.2			11,956.33	7.7		
	2	12,503.44	2.2			12,342.37	7.6		
	3	11,956.33	2.2			12,503.44	7.5		
	4	12,760.66	2.2			11,640.72	7.4		
41 <sup>†</sup>	5	12,772.78	2.2			12,760.66	7.0		
	1	13,404.77	1.7			13,145.71	4.7		
	2	13,145.71	1.7			13,012.2	4.7		
	3	13,515.2	1.7			12,982.38	4.7		

(continued on next page)

**Table 3** (continued)

$A^+ + K \rightarrow A(k) + K^+$									
40 keV									
$A^+$	Initial (0.0 cm)			Final (120.0 cm)			5 keV		
(Z)	#	Level (cm <sup>-1</sup> )	%	Level (cm <sup>-1</sup> )	%	Level (cm <sup>-1</sup> )	%	Level (cm <sup>-1</sup> )	%
42	4	13,629.15	1.7			13,404.77	4.6		
	5	13,012.2	1.7			12,692.12	4.6		
	1	16,641.081	3.3	0.0	5.2	16,641.081	12.8	16,641.081	13.1
	2	16,692.905	3.3	16,692.905	3.9	16,692.905	12.5	16,692.905	12.9
	3	16,747.72	3.3	16,747.72	3.9	16,747.72	12.2	16,747.72	12.6
	4	16,783.856	3.3	16,641.081	3.9	16,783.856	12.1	16,783.856	12.4
43	5	16,784.522	3.3	16,783.856	3.9	16,784.522	12.1	16,784.522	12.4
	1	16,287.79	2.4	16,428.71	4.7	16,025.15	6.1	16,428.71	10.4
	2	16,133.98	2.4	16,874.51	4.7	16,133.98	6.1	16,874.51	9.1
	3	16,025.15	2.4	17,522.92	4.6	15,770.42	6.1	17,522.92	6.6
	4	16,415.64	2.4	0.0	4.5	16,287.79	6.0	16,025.15	5.4
44	5	16,428.71	2.4	16,287.79	2.4	15,624.25	5.9	16,133.98	5.4
	1	17,096.87	2.8	0.0	3.5	17,096.87	12.6	17,096.87	18.6
	2	17,045.97	2.8	17,096.87	3.2	17,045.97	12.3	16,240.13	12
	3	16,712.58	2.8	16,240.13	3	16,712.58	10.6	16,712.58	11.2
45	4	16,240.13	2.7	15,550.16	2.8	16,240.13	8.1	16,190.61	8.3
	5	20,055.71	2.7	1190.64	2.6	16,190.61	7.8	15,550.16	7.6
	1	16,943.5	6.9	16,943.5	11.3	16,943.5	26.4	16,943.5	36.7
	2	16,120.72	6.3	16,118.69	10.3	16,120.72	15.0	16,118.69	20.8
	3	16,118.69	6.3	0.0	9.4	16,118.69	15.0	16,120.72	10.4
46	4	16,017.94	6.2	14,787.87	8.4	16,017.94	13.9	16,017.94	9.6
	5	14,787.87	5.2	12,723.07	5.7	14,787.87	5.7	14,787.87	7.9
	1	25,101.235	20.3	25,101.235	25.2	25,101.235	62.9	25,101.235	63.6
	2	28,213.767	18.3	28,213.767	22.7	28,213.767	27.0	28,213.767	27.3
	3	29,711.109	14.7	29,711.109	18.2	29,711.109	7.5	29,711.109	7.5
47	4	34,068.977	5.5	6564.148	8.4	34,068.977	0.5	6564.148	0.4
	5	35,041.751	4.3	34,068.977	3.7	35,041.751	0.3	34,068.977	0.3
	1	29,552.05741	29.6	0.0	59.1	29,552.05741	34.8	0.0	62.9
	2	30,242.29835	24.7	30,242.29835	24.7	30,242.29835	26.2	30,242.29835	26.2
	3	30,472.66516	23.2	34,714.22643	7.9	30,472.66516	23.9	34,714.22643	5.7
48	4	34,714.22643	7.9	42,556.147	1.5	34,714.22643	5.7	42,556.147	0.9
	5	0.0	4.3	51,886.965	0.3	0.0	2.9	51,886.965	0.2
	1	31,826.952	31.8	31,826.952	32.7	30,656.087	36.4	0.0	36.3
	2	30,656.087	31.7	30,113.99	32	31,826.952	33.6	31,826.952	33.7
	3	30,113.99	30.8	0.0	28.5	30,113.99	29.9	30,113.99	29.9
49	4	43,692.384	2.4	30,656.087	5.1	43,692.384	0.0	30,656.087	0.2
	5	51,483.98	0.4	58,390.9	0.1	51,483.98	0.0	53,310.101	0
	1	2212.599	56.8	2212.599	57.1	2212.599	83.3	2212.599	83.4
	2	0.0	36.9	0.0	38.3	0.0	16.2	0.0	16.3
	3	24,372.957	1	31,816.982	0.2	24,372.957	0.1	31,816.982	0
50	4	31,816.982	0.2	32,115.251	0.2	31,816.982	0.0	32,115.251	0
	5	32,115.251	0.2	34,977.678	0.2	32,115.251	0.0	34,977.678	0
	1	17,162.499	67.5	17,162.499	26.1	17,162.499	99.1	17,162.499	95.4
	2	8612.955	12.4	1691.806	15.7	8612.955	0.4	8612.955	1.3
	3	3427.673	3.5	8612.955	14.5	3427.673	0.1	1691.806	0.9
51	4	1691.806	2.4	3427.673	13.9	1691.806	0.1	3427.673	0.8
	5	0.0	1.7	0.0	11.4	0.0	0.0	0.0	0.7
	1	18,464.202	35.9	18,464.202	29.5	18,464.202	46.4	18,464.202	39.9
	2	16,395.359	21.2	0.0	19.1	16,395.359	21.6	16,395.359	18.5
	3	43,249.337	6.3	16,395.359	17.5	43,249.337	5.0	0.0	15.7
52	4	9854.018	4.8	9854.018	5.5	9854.018	3.8	9854.018	4.5
	5	8512.125	3.6	8512.125	5.4	8512.125	2.9	8512.125	4.5
	1	23,198.392	50.3	0.0	30.8	23,198.392	69.4	23,198.392	37.2
	2	44,253.0	11	23,198.392	21	44,253.0	7.5	0.0	26.8
	3	46,652.738	5.7	54,160.094	2.2	46,652.738	3.6	54,160.094	1.7
53	4	10,557.877	2.7	54,199.122	2.1	10,557.877	1.7	54,199.122	1.7
	5	4750.712	1.1	54,535.345	2	4750.712	0.7	54,535.345	1.6
	1	54,633.46	20.8	0.0	36.2	54,633.46	24.5	0.0	41.2
	2	56,092.881	13.6	7602.97	5	56,092.881	14.8	7602.97	5
	3	60,896.243	3.8	63,186.758	2.4	60,896.243	3.8	63,186.758	2.4
54	4	61,819.779	3.1	64,906.29	1.7	61,819.779	3.1	64,906.29	1.7
	5	63,186.758	2.3	64,989.994	1.6	63,186.758	2.3	64,989.994	1.6
	1	67,067.547	24.3	67,067.547	27.9	67,067.547	27.5	67,067.547	31.2
	2	68,045.156	18.2	0.0	23.4	68,045.156	19.3	0.0	24.3
	3	76,196.767	2.2	76,196.767	1.8	76,196.767	2.2	76,196.767	1.8
55	4	77,185.041	1.8	78,403.061	1.7	77,185.041	1.8	78,403.061	1.6
	5	77,269.145	1.8	78,119.798	1.6	77,269.145	1.7	78,119.798	1.5
	1	0.0	56.8	0.0	68.1	0.0	62.1	0.0	72.8
	2	11,178.26816	3.3	18,535.5286	0.9	11,178.26816	2.9	18,535.5286	0.8

(continued on next page)

**Table 3** (continued)

$A^+ + K \rightarrow A(k) + K^+$								
40 keV								
$A^+$		Initial (0.0 cm)		Final (120.0 cm)		5 keV		
(Z)	#	Level (cm <sup>-1</sup> )	%	Level (cm <sup>-1</sup> )	%	Level (cm <sup>-1</sup> )	%	Level (cm <sup>-1</sup> )
56	3	11,732.3071	2.9	22,588.821	0.5	11,732.3071	2.6	22,588.821
	4	14,499.2568	1.7	22,631.6863	0.5	14,499.2568	1.6	22,631.6863
	5	14,596.84232	1.7	24,317.1494	0.4	14,596.84232	1.5	24,317.1494
	1	0.0	48.8	0.0	27	0.0	98.3	0.0
	2	9033.966	9.1	9033.966	15.7	9033.966	0.4	9033.966
57 <sup>†</sup>	3	9215.501	8.6	9215.501	14.8	9215.501	0.3	9215.501
	4	9596.533	7.7	9596.533	12.8	9596.533	0.3	9596.533
	5	11,395.35	4.5	12,266.024	5.8	11,395.35	0.1	12,266.024
	1	3494.526	7.2			3494.526	22.8	
	2	4121.572	7.1			3010.002	20.7	
58 <sup>†</sup>	3	3010.002	7.1			4121.572	20.4	
	4	2668.188	6.9			2668.188	17.8	
	5	1053.164	5.7			1053.164	5.3	
	1	3312.24	1.2			3210.583	4.2	
	2	3210.583	1.2			3196.607	4.2	
59 <sup>†</sup>	3	3196.607	1.2			3312.24	4.1	
	4	3100.151	1.2			3100.151	4.1	
	5	3710.513	1.2			3710.513	3.9	
	1	2846.75	3.6			2846.75	25.3	
	2	1376.6	3.3			1376.6	14.9	
60	3	4381.1	3.3			4381.1	11.5	
	4	4432.22	3.3			4432.22	11.0	
	5	4866.54	3.1			4866.54	7.6	
	1	3681.696	3.8	3681.696	3.3	3681.696	28.7	3681.696
	2	2366.597	3.7	2366.597	3.2	2366.597	26.3	2366.597
61 <sup>†</sup>	3	5048.602	3.4	5048.602	2.9	5048.602	11.5	5048.602
	4	1128.056	3.3	1128.056	2.8	1128.056	10.9	1128.056
	5	0.0	2.7	0.0	2.5	0.0	4.2	0.0
	1	3919.03	9			3919.03	22.6	
	2	2797.1	8.7			2797.1	19.1	
62	3	5089.79	8.4			5089.79	11.9	
	4	5249.48	8.3			5249.48	10.5	
	5	5460.5	8.1			1748.78	9.2	
	1	4020.66	7.1	4020.66	7.1	4020.66	37.9	4020.66
	2	3125.46	6.8	3125.46	6.7	3125.46	27.7	3125.46
63	3	2273.09	6.1	2273.09	6.1	2273.09	14.5	2273.09
	4	1489.55	5.4	1489.55	5.4	1489.55	7.2	1489.55
	5	811.92	4.7	811.92	4.7	811.92	3.9	811.92
	1	0.0	19.1	0.0	46.4	0.0	60.7	0.0
	2	12,923.72	5.6	15,137.72	4.7	12,923.72	3.4	15,137.72
64	3	13,048.9	5.4	15,248.76	4.6	13,048.9	3.2	15,248.76
	4	13,222.04	5.1	15,421.25	4.5	13,222.04	2.9	15,421.25
	5	13,457.21	4.8	15,680.28	4	13,457.21	2.7	15,680.28
	1	8498.434	2.8	10,222.233	4	7947.294	9.3	7653.927
	2	7947.294	2.8	10,359.905	3.9	8498.434	9.1	7562.457
65 <sup>†</sup>	3	7653.927	2.8	10,576.41	3.8	7653.927	8.6	7426.71
	4	7562.457	2.8	10,883.505	3.6	7562.457	8.3	7234.91
	5	7480.348	2.8	7653.927	3.6	7480.348	8.0	6976.508
	1	5829.86	2.2			5829.86	6.0	
	2	6259.09	2.1			5483.98	5.7	
66	3	6351.75	2.1			6259.09	5.6	
	4	6488.28	2.1			5425.06	5.6	
	5	5483.98	2.1			6351.75	5.5	
	1	7050.603	8.5	7050.603	9.3	7050.603	35.2	7050.603
	2	7565.61	8.2	7565.61	9	7565.61	25.9	7565.61
67	3	8519.21	7.3	8519.21	8.1	8519.21	11.5	8519.21
	4	4134.222	6.7	4134.222	7.8	4134.222	9.1	4134.222
	5	9211.591	6.5	9211.591	7.1	9211.591	6.0	9211.591
	1	8605.16	22.6	8605.16	24.5	8605.16	49.2	8605.16
	2	5419.7	21.3	5419.7	23	5419.7	40.5	5419.7
68	3	10,695.75	15.2	10,695.75	16.5	10,695.75	7.0	10,695.75
	4	13,094.42	7.5	0.0	6.7	13,094.42	1.1	0.0
	5	0.0	5.3	13,094.42	4.4	0.0	0.6	13,094.42
	1	6958.329	18.7	6958.329	20.9	6958.329	69.7	6958.329
	2	10,750.982	14	10,750.982	15.6	5035.193	13.0	10,750.982
69	3	5035.193	13.9	5035.193	9.8	10,750.982	10.9	5035.193
	4	12,377.534	9.2	12,377.534	6.5	12,377.534	2.5	12,377.534
	5	13,097.906	7.4	13,097.906	5.2	13,097.906	1.4	13,097.906
	1	8771.243	63.7	8771.243	60.7	8771.243	99.1	8771.243

(continued on next page)

**Table 3** (continued)

$A^+ + K \rightarrow A(k) + K^+$									
40 keV									
$A^+$		Initial (0.0 cm)		Final (120.0 cm)		5 keV			
(Z)	#	Level ( $\text{cm}^{-1}$ )	%						
70	2	0.0	8.9	0.0	10.5	0.0	0.3	0.0	0.3
	3	20,406.84	2.5	22,419.764	2.2	20,406.84	0.1	22,419.764	0
	4	21,799.38	1.6	22,559.502	2.1	21,799.38	0.0	22,559.502	0
	5	22,419.764	1.3	20,406.84	2.1	22,419.764	0.0	20,406.84	0
	1	17,288.439	26.7	0.0	36.3	17,288.439	28.6	0.0	37.3
	2	0.0	23.2	17,288.439	33	0.0	25.5	17,288.439	35.8
71	3	17,992.007	20.9	19,710.388	14.2	17,992.007	20.6	19,710.388	12.9
	4	19,710.388	11.5	24,489.102	3.2	19,710.388	10.3	24,489.102	2.9
	5	24,489.102	2.6	24,751.948	3	24,489.102	2.3	24,751.948	2.7
	1	1993.92	31.1	1993.92	31.6	1993.92	63.4	1993.92	63.4
	2	4136.13	27.5	4136.13	27.6	4136.13	21.9	4136.13	21.9
72	3	0.0	24.2	0.0	25.7	0.0	13.6	0.0	13.6
	4	7476.39	11.7	7476.39	11.7	7476.39	1.0	7476.39	1
	5	17,427.28	0.4	18,851.31	0.3	17,427.28	0.0	18,851.31	0
	1	14,017.83	6.9	14,092.28	9.3	14,017.83	19.6	14,092.28	22.9
	2	14,092.28	6.9	14,740.68	8.9	14,092.28	19.1	14,017.83	17.7
73	3	14,435.13	6.8	15,673.33	7.8	14,435.13	15.9	14,740.68	15.3
	4	14,541.68	6.7	14,017.83	7	14,541.68	14.8	14,435.13	14.3
	5	14,740.68	6.6	14,435.13	6.8	14,740.68	12.7	14,541.68	13.3
	1	19,657.78	2.7	0.0	6.3	19,657.78	10.2	0.0	12.8
	2	19,178.45	2.7	20,646.54	3.7	19,178.45	10.1	19,657.78	12.1
74	3	20,340.39	2.6	21,153.33	3.5	20,340.39	7.5	20,646.54	9.9
	4	20,560.26	2.6	21,622.92	3.2	18,504.72	7.2	19,178.45	8.4
	5	18,504.72	2.5	23,355.41	3.2	20,560.26	6.4	21,153.33	6.2
	1	22,476.68	2.6	2951.29	8.9	22,476.68	8.5	1670.29	19.4
	2	21,453.9	2.6	1670.29	8.6	21,453.9	8.4	0.0	10.2
75 <sup>†</sup>	3	21,448.76	2.6	0.0	6.4	21,448.76	8.3	22,476.68	9.4
	4	22,773.78	2.6	4830.0	4.8	22,773.78	7.3	23,047.31	9.3
	5	22,852.8	2.6	23,047.31	4.3	22,852.8	6.9	22,773.78	8.1
	1	21,775.4	4.9			21,775.4	17.0		
	2	22,160.04	4.9			22,160.04	15.7		
76 <sup>†</sup>	3	22,422.83	4.8			22,422.83	13.9		
	4	23,154.81	4.5			20,481.73	9.0		
	5	20,481.73	4.5			20,447.8			
	1	25,601.55	3.8			25,601.55	10.8		
	2	25,593.94	3.8			25,593.94	10.7		
77	3	27,954.32	3.8			27,954.32	8.2		
	4	28,139.52	3.7			25,275.42	8.1		
	5	25,275.42	3.7			28,139.52	6.8		
	1	30,529.66	6	0.0	27.7	30,529.66	32.3	30,529.66	29.7
	2	32,463.58	5.5	7106.61	8.5	32,463.58	13.0	7106.61	16.1
78 <sup>†</sup>	3	32,513.43	5.4	5784.62	8.2	32,513.43	12.4	0.0	15.5
	4	32,830.78	5.1	32,830.78	7	32,830.78	8.9	5784.62	12.4
	5	33,064.83	4.9	2834.98	6.5	33,064.83	7.0	32,830.78	11.5
	1	30,157.0	31.3			30,157.0	93.2		
	2	26,638.6	14.9			26,638.6	3.4		
79	3	36,296.4	10			36,296.4	1.1		
	4	36,781.6	8.5			36,781.6	0.7		
	5	38,536.2	4.6			38,536.2	0.3		
	1	37,358.991	51.5	0.0	65.4	37,358.991	80.6	0.0	87.3
	2	41,174.613	13.8	42,163.53	9.8	41,174.613	6.6	42,163.53	4.1
80	3	42,163.53	9.8	21,435.191	5.5	42,163.53	4.1	21,435.191	2.2
	4	21,435.191	5.5	45,537.195	3.3	21,435.191	2.2	45,537.195	1.1
	5	45,537.195	3.3	46,174.979	2.7	45,537.195	1.1	46,174.979	0.9
	1	44,042.909	47.6	44,042.909	48.7	44,042.909	85.9	44,042.909	86
	2	39,412.237	29.9	0.0	31.4	39,412.237	11.3	0.0	11.4
81	3	37,644.982	17.6	37,644.982	18.5	37,644.982	2.6	37,644.982	2.6
	4	54,068.6829	2.1	71,336.005	0	54,068.6829	0.1	71,336.005	0
	5	62,350.325	0.2	70,932.2	0	62,350.325	0.0	76,466.936	0
	1	7792.7	86.3	7792.7	86.4	7792.7	99.7	7792.7	99.7
	2	0.0	12	0.0	12.6	0.0	0.3	0.0	0.3
82	3	26,477.5	0.5	34,159.9	0.1	26,477.5	0.0	34,159.9	0
	4	34,159.9	0.1	35,161.1	0.1	34,159.9	0.0	35,161.1	0
	5	35,161.1	0.1	41,368.1	0	35,161.1	0.0	46,949.9	0
	1	45,443.171	6.2	10,650.3271	11.4	45,443.171	5.9	10,650.3271	10.6
	2	46,060.8364	5.6	7819.2626	5.7	46,060.8364	5.3	7819.2626	5.6
	3	46,068.4385	5.6	0.0	5.6	46,068.4385	5.3	0.0	5.3
	4	46,328.6668	5.3	52,101.66	2.1	46,328.6668	5.1	52,101.66	2.1
	5	52,101.66	2.1	52,311.315	2.1	52,101.66	2.1	52,311.315	2.1

(continued on next page)

**Table 3** (continued)

$A^+ + K \rightarrow A(k) + K^+$									
40 keV									
$A^+$		Initial (0.0 cm)		Final (120.0 cm)		5 keV			
(Z)	#	Level (cm <sup>-1</sup> )	%						
83	1	15,437.501	52.6	15,437.501	52.9	15,437.501	90.2	15,437.501	90.2
	2	21,660.914	28	21,660.914	28.1	21,660.914	7.2	21,660.914	7.2
	3	11,419.039	16.4	11,419.039	16.6	11,419.039	2.5	11,419.039	2.5
	4	32,588.221	0.8	0.0	0.9	32,588.221	0.0	0.0	0.1
	5	0.0	0.7	33,164.805	0.7	0.0	0.0	33,164.805	0
84 <sup>†</sup>	1	21,679.11	70.9			21,679.11	89.9		
	2	16,831.61	14.8			16,831.61	5.8		
	3	39,081.19	4.9			39,081.19	1.5		
	4	40,802.7	3			40,802.7	0.9		
	5	42,718.0	1.8			42,718.0	0.5		
85 <sup>†</sup>									
86 <sup>†</sup>	1	54,620.35	45.5			54,620.35	49.2		
	2	55,989.03	28			55,989.03	27.6		
	3	66,244.97	1.8			66,244.97	1.6		
	4	66,707.53	1.6			66,707.53	1.4		
	5	67,906.52	1.3			67,906.52	1.1		
87	1	0.0	78.4	0.0	88.7	0.0	83.1	0.0	91.7
	2	12,237.409	2.4	16,229.87	1.4	12,237.409	1.9	16,229.87	1.2
	3	13,923.998	1.7	16,429.64	1.3	13,923.998	1.3	16,429.64	1.1
	4	16,229.87	1.1	19,739.98	0.9	16,229.87	0.9	19,739.98	0.9
	5	16,429.64	1.1	30,936.325	0.1	16,429.64	0.8	30,936.325	0.1
88 <sup>‡</sup>									
89	1	2231.43	43.2			2231.43	80.4		
	2	0.0	34			0.0	18.8		
	3	9217.28	5.5			9217.28	0.2		
	4	9863.59	4.3			9863.59	0.1		
	5	10,000.0	4			10,000.0	0.1		

compared to the direct population of the lower state of an atomic transition is taken from the kinetic energy of the beam. This energy difference gives a Doppler shift away from the transition frequency to a portion of the atoms in the subsequent beam with respect to those which react to directly populate the lower state.

This can be shown by comparing the beam energy before the reaction  $T_{B,I}$  with that after the reaction  $T_{B,II}$  with an IP energy difference of  $\Delta E = I_A - I_B$

$$T_{B,II} = T_{B,I} - \Delta E \quad (13)$$

for the intermediate state reaction this becomes

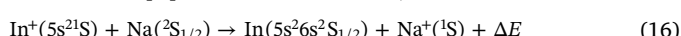
$$T_{B,II}^* = T_{B,I} - \Delta E - E^* \quad (14)$$

therefore the relative energy difference between these two product atom beams is given by the intermediate state excitation energy  $E^*$

$$\Delta T_{B,II}^* = E^* . \quad (15)$$

The de-excitation of these intermediate states occurs by spontaneous emission isotropically before that population is accessible from the lower state [70], therefore the sidepeak amplitude is a function of time from charge exchange. Inelastic collisional excitation following charge exchange to these intermediate states can have the same effect [71], this contribution is discussed later.

As the population passing through intermediate states was recorded in the simulation, the resulting contribution to the peak shape can also be simulated. The hyperfine structure resonances were modelled with a Voigt line profile [72], with the intermediate populations as sidepeaks detuned by the corresponding frequency. As an example, Fig. 6 shows both the calculated detuned population and the corresponding peak shape function for the transition at 246.0 nm. The largest contribution to this is from population of the  $5s^26s^2S_{1/2}$  state at 24372.957 cm<sup>-2</sup>, via



which then de-excites to the ground state



where  $E_\gamma^* = 3.021$  eV is the additional kinetic energy from the ion beam which is required for this reaction compared to the direct population of the  $5s^26s^2S_{1/2}$  state, corresponding to a Doppler shift of 40 MHz for the transition frequency.

As the many detuned population contributions were not fully resolvable with the 34 MHz spectral linewidth of the laser used, only this largest indirect contribution was left as a free parameter in the fitting, with the others fixed proportional the simulated relative populations.

For the 246.0-nm and 246.8-nm transitions the fitted sidepeak amplitudes were determined to be 13.95(144)% (shown in Fig. 6) and 5.7(27)% respectively, an average over 5 hyperfine spectra of each. The dominant sidepeak amplitudes from simulation were determined to be 3.8% and 0.5%, with the largest contribution for both transitions from the  $5s^26s^2S_{1/2}$  state. The additional contribution can be attributed to inelastic collisions, primarily with the sodium vapour in the poorer vacuum region of the charge-exchange cell.

Often inelastic collisions are attributed to observed tails in hyperfine structure peaks, where Poisson's law can be taken as the ratio of sidepeak heights of a series of equally spaced peaks from the order of the inelastic collisions [71]. As the  $5s^26s^2S_{1/2}$  state is also the first excited state after the  $^2P_{1/2}$  and  $^2P_{3/2}$  states of interest, the relative contribution from the inelastic collisions were determined to be 10.14(144)% and 5.2(27)% respectively. As the inelastic contribution increases, the ratio of the sidepeak amplitudes between the  $^2P_{1/2}$  and  $^2P_{3/2}$  states will become closer compared to the original prediction of 3.8% and 0.5%. Alternatively, population of unknown states during charge-exchange which decay to the  $^2P_{1/2}$  and  $^2P_{3/2}$  states could be responsible for the additional contribution to the sidepeak amplitude.

Inelastic collisions are the most likely mechanism in the case of symmetric charge exchange (e.g.  $Na^+ + Na$ ) at low  $T_B$ , but for asymmetric charge exchange the sidepeaks intrinsic to the de-excitation following charge exchange will always be present with the additional

**Table 4**

Total cross-sections  $\sigma_{CE}$  for neutralisation of an ion beam of elements  $A = 1\text{--}90$  by free K or Na atoms. Atomic data sourced from the NIST atomic database [48]  
<sup>‡</sup> - insufficient level data was available to provide reliable values for these elements.

Total cross-section $\sigma_{CE}(\text{cm}^2)$				
$A^+(Z)$	$A^+ + K \rightarrow A + K^+$		$A^+ + Na \rightarrow A + Na^+$	
	40 keV	5 keV	40 keV	5 keV
1	3.7e-13	1.1e-13	3.0e-13	7.0e-14
2	4.0e-13	5.6e-14	2.8e-13	3.1e-14
3	1.2e-13	1.5e-14	7.6e-14	9.8e-15
4	1.3e-13	1.2e-14	8.8e-14	7.5e-15
5	8.9e-14	2.0e-14	6.1e-14	1.6e-14
6	2.7e-13	3.0e-14	1.7e-13	8.4e-15
7	2.8e-13	4.8e-14	1.7e-13	1.2e-14
8	1.2e-13	1.7e-14	7.1e-14	5.3e-15
9	1.3e-13	3.8e-14	7.3e-14	2.0e-14
10	1.2e-13	2.0e-14	6.8e-14	2.3e-14
11	2.8e-14	2.6e-15	1.7e-14	7.1e-15
12	5.2e-14	9.8e-15	3.5e-14	1.9e-14
13	2.8e-14	9.3e-16	1.9e-14	2.8e-15
14	7.3e-14	8.0e-15	4.0e-14	1.7e-15
15	1.1e-13	5.7e-15	5.2e-14	1.0e-15
16	5.2e-14	4.6e-15	2.6e-14	6.3e-16
17	8.9e-14	1.9e-14	4.2e-14	1.7e-15
18	6.3e-14	2.4e-14	3.1e-14	1.6e-15
19	2.0e-14	9.0e-15	1.1e-14	9.1e-16
20	6.5e-14	2.8e-14	3.4e-14	2.5e-15
21	2.7e-13	1.9e-13	1.6e-13	6.5e-14
22	6.2e-13	2.9e-13	3.7e-13	1.4e-13
23	6.7e-13	3.5e-13	4.1e-13	1.5e-13
24	3.4e-13	9.8e-14	1.4e-13	1.2e-14
25	2.2e-13	1.2e-13	1.3e-13	6.7e-14
26	6.3e-13	2.5e-13	4.5e-13	2.5e-13
27	4.3e-13	1.9e-13	2.9e-13	1.2e-13
28	2.6e-13	1.3e-13	1.3e-13	1.6e-14
29	2.8e-14	5.0e-15	1.5e-14	6.2e-16
30	1.8e-14	1.1e-15	2.1e-14	1.6e-14
31	6.4e-15	1.3e-16	8.2e-15	7.6e-16
32	1.3e-14	3.1e-16	8.2e-15	5.3e-16
33	1.8e-14	6.5e-16	5.8e-15	1.1e-16
34	1.2e-14	1.1e-15	4.5e-15	1.1e-16
35	2.6e-14	3.6e-15	7.5e-15	2.1e-16
36	2.5e-14	6.9e-15	7.9e-15	2.1e-16
37	1.0e-14	6.8e-15	3.7e-15	1.3e-16
38	3.0e-14	4.3e-15	1.2e-14	9.6e-16
39	2.2e-13	1.6e-13	9.5e-14	2.2e-14
40	5.0e-13	2.5e-13	2.8e-13	1.1e-13
41	5.7e-13	2.7e-13	3.6e-13	1.8e-13
42	4.1e-13	1.6e-13	1.9e-13	5.7e-14
43	4.0e-13	2.1e-13	2.6e-13	1.4e-13
44	3.6e-13	1.4e-13	2.2e-13	5.7e-14
45	1.2e-13	4.1e-14	8.3e-14	1.7e-14
46	7.3e-14	1.5e-14	3.1e-14	1.2e-14
47	1.7e-14	2.5e-15	3.7e-15	8.7e-17
48	1.1e-14	5.9e-16	2.0e-14	2.3e-14
49	2.9e-15	6.2e-17	8.4e-15	1.9e-15
50	5.7e-15	1.5e-16	9.2e-15	7.8e-15
51	3.6e-15	8.0e-17	2.8e-15	7.0e-17
52	5.3e-15	1.6e-16	2.8e-15	8.6e-17
53	8.7e-15	3.6e-16	2.2e-15	4.1e-17
54	1.1e-14	6.7e-16	2.5e-15	4.5e-17
55	6.1e-15	7.3e-16	1.3e-15	2.4e-17
56	3.8e-14	8.6e-15	1.3e-14	8.1e-15
57	2.0e-13	7.4e-14	9.2e-14	3.9e-14
58	1.4e-12	5.3e-13	5.6e-13	2.2e-13
59	6.3e-13	2.8e-13	1.9e-13	3.5e-14
60	7.3e-13	2.7e-13	1.7e-13	2.8e-14
61	7.9e-14	1.0e-14	7.5e-14	3.9e-14
62	3.6e-13	6.5e-14	9.6e-14	2.4e-14
63	9.1e-14	1.2e-14	1.9e-14	6.2e-16
64	6.4e-13	2.6e-13	2.4e-13	9.6e-14
65	4.5e-13	2.6e-13	3.1e-13	1.5e-13
66	2.4e-13	9.5e-14	7.8e-14	2.3e-14
67	6.9e-14	1.9e-14	2.7e-14	8.9e-15

**Table 4 (continued)**

Total cross-section $\sigma_{CE}(\text{cm}^2)$				
$A^+(Z)$	$A^+ + K \rightarrow A + K^+$		$A^+ + Na \rightarrow A + Na^+$	
	40 keV	5 keV	40 keV	5 keV
68	8.8e-14	1.1e-14	3.4e-14	9.8e-15
69	2.0e-14	4.8e-16	1.1e-14	8.8e-15
70	1.9e-14	4.6e-15	3.2e-15	6.8e-17
71	1.7e-14	5.7e-15	2.1e-14	1.4e-14
72	2.0e-13	7.5e-14	9.7e-14	4.4e-14
73	4.5e-13	2.5e-13	2.5e-13	9.0e-14
74	4.4e-13	2.5e-13	2.6e-13	9.9e-14
75	2.4e-13	1.4e-13	1.4e-13	5.5e-14
76	2.1e-13	6.0e-14	1.7e-13	5.5e-14
77	2.5e-13	1.1e-13	1.1e-13	2.7e-14
78	6.8e-14	2.8e-14	2.2e-14	8.2e-15
79	2.6e-14	6.2e-15	6.1e-15	2.6e-16
80	6.8e-15	2.7e-16	1.4e-14	5.4e-15
81	2.0e-15	5.4e-17	8.2e-15	9.5e-15
82	2.3e-16	1.9e-18	1.1e-16	3.7e-19
83	8.6e-15	2.0e-15	1.1e-14	2.7e-15
84	3.4e-15	7.0e-17	3.7e-15	1.7e-16
85 <sup>‡</sup>				
86	8.7e-15	8.3e-16	9.5e-16	1.4e-17
87	6.6e-15	1.6e-15	7.2e-16	1.2e-17
88 <sup>‡</sup>				
89	3.9e-14	1.6e-14	1.6e-14	1.1e-14

contribution to the peaks from these inelastic collisions. As potassium has a lower IP than sodium the sidepeak contribution from de-excitation after charge exchange is expected to be much larger for  $In^+$  neutralised by potassium, as a higher proportion of high-lying states will be populated, this is visible in Fig. 1.

## 5. Summary

Simulations were performed of the relative atomic population distribution of ion beams of elements  $1 \leq Z \leq 89$ , following neutralisation by potassium and sodium vapours, at incident beam energies of 5 and 40 keV. This was achieved by calculating neutralisation cross sections using a semi-classical impact-parameter approach [5] and simulation of the subsequent population decay. In order to test the validity of the approach, measurements of the relative population of the ground and lowest-lying metastable states of indium were made using the CRIS setup. The relative populations were measured and simulated at an intermediate beam energy of 20 keV and found to be in agreement with the calculations. Further simulations were made to compare to other available experimental data in literature, overall agreement is good, with a possible explanation for a discrepancy suggested.

The simulations of elements elements  $1 \leq Z \leq 89$  were made with available atomic data from the NIST atomic database [48], the results are shown in Tables 2 and 3 for potassium and sodium neutralising vapours respectively. The results are given for the initial population distribution (at 0 cm) and for the final population distribution (at 120 cm) for beam energies of 5 keV and 40 keV. The five most highly populated states are listed in these tables. Collinear laser spectroscopy experiments are typically performed in this energy range, for which experimental data is extremely sparse. The simulations performed in this work will allow for inference of the atomic populations available in a range of experimental scenarios.

The use of a high-resolution injection-locked Ti:Sa laser and the large energy level spacing between the ground, lowest metastable state, and next highest states allowed for detuned contributions to atomic transition lineshapes to be partially resolvable. The contribution to the lineshapes from the neutralisation process was also simulated and compared.

The feasibility of the CRIS technique for measuring relative atomic

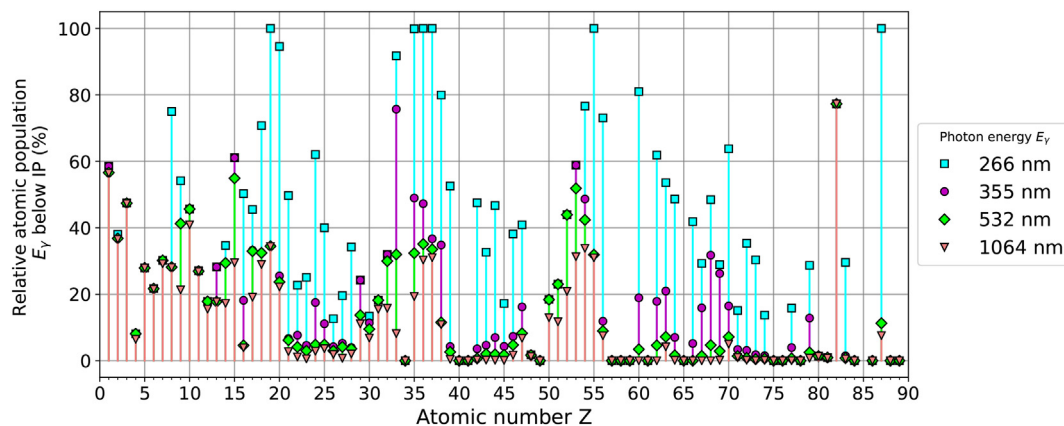


**Fig. 5.** Calculated fraction of atomic population within  $E_\gamma$  of the ionization potential of elements  $1 \leq Z \leq 89$ , where  $E_\gamma$  is the energy of the non-resonant ionization photon. Cross-sections were calculated for a 40 keV ion beam neutralised by sodium vapour. Populations are after 120 cm of flight. Where insufficient line data was available only the initial population at 0 cm is given. No values are reported for elements with insufficient level information available.

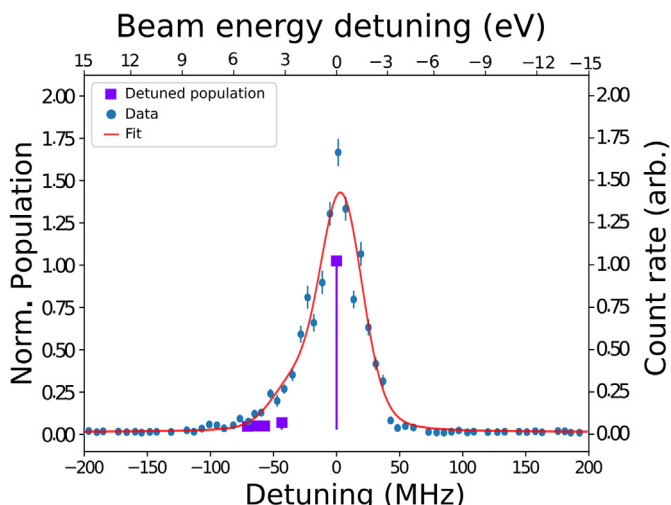


**Fig. 6.** For measurements with the 246.0-nm transition  $^2\text{P}_{1/2} \rightarrow 8\text{s } ^2\text{S}_{1/2}$ . The calculated detuned population (purple) overlayed with an example atomic transition peak of the hyperfine structure of  $^{115}\text{In}$ , fitted with free charge-exchange sidepeak amplitudes (red fit). (For interpretation of the references to colour in this figure legend, the reader is referred to the web version of this article.)

populations has been demonstrated with possible adaptations for improved measurements highlighted. The semi-classical approach by R&F [5], when combined with atomic population simulation has shown to provide reliable prediction of relative populations following charge exchange, even for three-electron systems like indium. The calculations compiled here will be of use to future CLS experiments where prediction of atomic population is crucial for developing efficient laser schemes.

## Acknowledgements

This work was supported by ERC Consolidator Grant No.648381 (FNPMILS); STFC grants ST/L005794/1 and ST/L005786/1 and Ernest Rutherford Grant No. ST/L002868/1; GOA 15/010 from KU Leuven; the FWO-Vlaanderen (Belgium) and the European Unions Seventh Framework Programme for Research and Technological Development under Grant Agreement 654,002 (ENSAR2). We acknowledge the financial aid from the Ed Schneiderman Fund at New York University. We also thank the University of Jyväskylä for the use of the injection-locked cavity.

## References

- [1] R.F. Garcia Ruiz, A.R. Vernon, C.L. Binnensley, B.K. Sahoo, M. Bissell, J. Billowes, T.E. Cocolios, W. Gins, R.P. de Groot, K.T. Flanagan, A. Koszorus, K.M. Lynch, G. Neyens, C.M. Ricketts, K.D.A. Wendt, S.G. Wilkins, X.F. Yang, High-precision multiphoton ionization of accelerated laser-ablated species, Phys. Rev. X 8 (4) (2018) 041005, , <https://doi.org/10.1103/PhysRevX.8.041005> URL.
- [2] K.T. Flanagan, K.M. Lynch, J. Billowes, M.L. Bissell, I. Budinčević, T.E. Cocolios, R.P. de Groot, S. De Schepper, V.N. Fedossev, S. Franchoo, R.F. Garcia Ruiz, H. Heylen, B.A. Marsh, G. Neyens, T.J. Procter, R.E. Rossel, S. Rothe, I. Strashnov, H.H. Stroke, K.D.A. Wendt, Collinear resonance ionization spectroscopy of neutron-deficient francium isotopes, Phys. Rev. Lett. 111 (21) (2013) 212501, , <https://doi.org/10.1103/PhysRevLett.111.212501> URL.
- [3] R. Catharella, W. Andreazza, M. Breitenfeldt, A. Dorsival, G.J. Focker, T.P. Gharsa, G. T. J., J.-L. Grenard, F. Locci, P. Martins, S. Marzari, J. Schipper, A. Shornikov, T. Stora, The ISOLDE facility, J. Phys. G Nucl. Part. Phys. 44 (9) (2017) 094002, <https://doi.org/10.1088/1361-6471/aa7eba> URL <http://stacks.iop.org/0954-3899/44/i=9/a=094002?key=crossref>.
- [4] S. Lukić, F. Gevaert, A. Kelić, M.V. Ricciardi, K.H. Schmidt, O. Yordanov, Systematic comparison of ISOLDE-SC yields with calculated in-target production rates, Nucl. Instruments Methods Phys. Res. Sect. A Accel. Spectrometers, Detect. Assoc. Equip. 565 (2) (2006) 784–800, <https://doi.org/10.1016/j.nima.2006.04.082>.
- [5] D. Rapp, W.E. Francis, Charge exchange between gaseous ions and atoms, J. Chem. Phys. 37 (11) (1962) 2631, <https://doi.org/10.1063/1.1733066> URL <http://scitation.aip.org/content/aip/journal/jcp/37/11/10.1063/1.1733066>.
- [6] A.W. Gianni Di Domenico, Vapor Pressure and Density of Alkali Metals, URL <https://demonstrations.wolfram.com/VaporPressureAndDensityOfAlkaliMetals/>.
- [7] A. Dalgaard, D.R. Bates, The mobilities of ions in their parent gases, Philos. Trans. R. Soc. A Math. Phys. Eng. Sci. 250 (1958) 426–439, <https://doi.org/10.1098/rsta.1958.0003> URL <http://rsta.royalsocietypublishing.org/cgi/doi/10.1098/rsta.1958.0003>.
- [8] Y.A. Kudriavtsev, V.S. Letokhov, Laser method of highly selective detection of rare radioactive isotopes through multistep photoionization of accelerated atoms, Appl. Phys. B Photophysics Laser Chem. 29 (3) (1982) 219–221, <https://doi.org/10.1007/BF00688671> URL <http://link.springer.com/10.1007/BF00688671>.
- [9] S.P. Freeman, R.P. Shanks, X. Donzel, G. Gaubert, Radiocarbon positive-ion mass spectrometry, Nucl. Instruments Methods Phys. Res. Sect. B Beam Interact. with Mater. Atoms 361 (2015) 229–232, <https://doi.org/10.1016/J.NIMB.2015.04.034> URL <https://www.sciencedirect.com/science/article/pii/S0168583X15003821>.
- [10] Y. Demkov, Quantum-Mechanical Calculation of the Probability of Charge-Exchange in Collisions, (1952).
- [11] A. Dalgaard, J.T. Lewis, Dipole and quadrupole polarizabilities of atoms and molecules, Proc. R. Soc. A Math. Phys. Eng. Sci. 240 (1221) (1957) 284–292, <https://doi.org/10.1098/rspa.1957.0084> URL <http://rspa.royalsocietypublishing.org/cgi/doi/10.1098/rspa.1957.0084>.
- [12] B.G. Lindsay, R.F. Stebbings, Charge transfer cross sections for energetic neutral atom data analysis, J. Geophys. Res. Sp. Phys. 110 (A12) (2005) 1–10, <https://doi.org/10.1029/2005JA011298>.
- [13] H.S.W. Massey, Collisions between atoms and molecules at ordinary temperatures, Rep. Prog. Phys. 12 (1) (1949) 311, <https://doi.org/10.1088/0034-4885/12/1/311> URL <http://stacks.iop.org/0034-4885/12/i=1/a=311?key=crossref>.
- [14] A.A. Sycheva, G.G. Balint-Kurti, A.P. Palov, Collision cross sections for O + Ar + collisions in the energy range 0.03500 eV, J. Phys. Chem. A 120 (27) (2016) 4655–4663, <https://doi.org/10.1021/acs.jpca.5b09151> URL <http://pubs.acs.org/doi/10.1021/acs.jpca.5b09151>.

- [org/doi/10.1021/acs.jpca.5b09151](https://doi.org/10.1021/acs.jpca.5b09151).
- [15] J.B. Hasted, Physics of Atomic Collisions, 2nd Edition, American Elsevier, 1972 URL <https://bibdata.princeton.edu/bibliographic/1917772>.
- [16] J.B.H. Stedeford, J.B. Hasted, Further investigations of charge exchange and electron detachment. I. Ion energies 3 to 40 keV. II. Ion energies 100 to 4000 eV, Proc. R. Soc. A Math. Phys. Eng. Sci. 227 (1955) 466–486, <https://doi.org/10.1098/rspa.1955.0024> URL <http://rspa.royalsocietypublishing.org/cgi/doi/10.1098/rspa.1955.0024>.
- [17] L. Vermeiren, R.E. Silverans, P. Lievens, A. Klein, R. Neugart, C. Schulz, F. Buchinger, Ultrasensitive radioactive detection of collinear-laser optical pumping: measurement of the nuclear charge radius of Ca 2, Phys. Rev. Lett. 68 (11) (1992) 1679–1682, <https://doi.org/10.1103/PhysRevLett.68.1679> URL <https://link.aps.org/doi/10.1103/PhysRevLett.68.1679>.
- [18] R.F. Garcia Ruiz, C. Gorges, M. Bissell, K. Blaum, W. Gins, H. Heylen, K. Koenig, S. Kaufmann, M. Kowalska, J. Krämer, P. Lievens, S. Malbrunot-Ettenuauer, R. Neugart, G. Neyens, W. Nörterhäuser, D.T. Yordanov, X.F. Yang, Development of a sensitive setup for laser spectroscopy studies of very exotic calcium isotopes, J. Phys. G Nucl. Part. Phys. 44 (4) (2017) 044003, , <https://doi.org/10.1088/1361-6471/aa5a24> URL <http://stacks.iop.org/0954-3899/44/i=4/a=044003?key=crossref.13fa0ab4b825db2b4775217790972cbc>.
- [19] A. Klose, K. Minamisono, C. Geppert, N. Frömingen, M. Hammen, J. Krämer, A. Krieger, C.D.P. Levy, P.F. Mantica, W. Nörterhäuser, S. Vinnikova, Tests of atomic charge-exchange cells for collinear laser spectroscopy, Nucl. Instruments Methods Phys. Res. Sect. A Accel. Spectrometers, Detect. Assoc. Equip. 678 (2012) 114–121, <https://doi.org/10.1016/j.nima.2012.03.006> (JUNE).
- [20] S. Paulo, A potassium charge exchange cell with recycling for negative ion source, Nucl. Inst. Methods 179 (1981) 195–198.
- [21] H.R. Hiddleston, Progress in Sodium Vapour Exchange (3), (1977), pp. 1600–1602.
- [22] W.M. Haynes, CRC Handbook of Chemistry and Physics: A Ready-Reference Book of Chemical and Physical Data, 96th Edition, CRC Press, Boulder, Colorado, USA, 2015.
- [23] H. Brinkman, H. Kramers, Zur Theorie der Einfangung von Elektronen durch  $\alpha$ -Teilchen, Proc. Acad. Sci. Amsterdam 8 (1930) 973.
- [24] E.F. Gurnee, J.L. Magee, Interchange of charge between gaseous molecules in resonant and Near $\alpha$  resonant processes, J. Chem. Phys. 26 (5) (1957) 1237–1248, <https://doi.org/10.1063/1.1743499> URL <http://aip.scitation.org/doi/10.1063/1.1743499>.
- [25] B.G. Lindsay, R.L. Merrill, H.C. Straub, K.A. Smith, R.F. Stebbings, Absolute differential and integral cross sections for charge transfer of keV O + with N 2, Phys. Rev. A 57 (1) (1998) 331–337, <https://doi.org/10.1103/PhysRevA.57.331> URL <https://link.aps.org/doi/10.1103/PhysRevA.57.331>.
- [26] I.Y. Tolstikhina, M.-Y. Song, M. Imai, Y. Iriki, A. Itoh, D. Kato, H. Tawara, J.-S. Yoon, V.P. Shevelko, Charge-changing collisions of tungsten and its ions with neutral atoms, J. Phys. B Atomic Mol. Phys. 45 (14) (2012) 145201, <https://doi.org/10.1088/0953-4075/45/14/145201> URL <http://stacks.iop.org/0953-4075/45/i=14/a=145201?key=crossref.228d8432aab161dea37dbf937b6bdd3a>.
- [27] D.P. Dewangan, J. Eichler, Charge exchange in energetic ion-atom collisions, Phys. Rep. 247 (2–4) (1994) 59–219, [https://doi.org/10.1016/0370-1573\(94\)90012-4](https://doi.org/10.1016/0370-1573(94)90012-4).
- [28] B.H. Bransden, M.R.C. McDowell, Charge Exchange and the Theory of Ion-Atom Collisions, Clarendon Press, 1992.
- [29] D. Dewangan, J. Eichler, Electron capture and the long range of the Coulomb interaction, Nucl. Instruments Methods Phys. Res. Sect. B Beam Interact. with Mater. Atoms 23 (1–2) (1987) 160–163, [https://doi.org/10.1016/0168-583X\(87\)90437-X](https://doi.org/10.1016/0168-583X(87)90437-X) URL <https://www.sciencedirect.com/science/article/pii/0168583X8790437X>.
- [30] J.R. Oppenheimer, On the quantum theory of the capture of electrons, Phys. Rev. 31 (3) (1928) 349–356, <https://doi.org/10.1103/PhysRev.31.349> URL <https://link.aps.org/doi/10.1103/PhysRev.31.349>.
- [31] J.S. Briggs, K. Dettmann, Radiative charge transfer from H atoms by fast ions, Phys. Rev. Lett. 33 (19) (1974) 1123–1125, <https://doi.org/10.1103/PhysRevLett.33.1123> URL <https://link.aps.org/doi/10.1103/PhysRevLett.33.1123>.
- [32] B. Najjari, A.B. Voitkiv, J. Ullrich, Mechanism for electron transfer in fast ion-atomic collisions, Phys. Rev. Lett. 101 (22) (2008) 1–4 arXiv:0808.0590 <https://doi.org/10.1103/PhysRevLett.101.223201>.
- [33] S. Sakabe, Y. Izawa, Cross sections for resonant charge transfer between atoms and their positive ions: collision velocity  $< = 1$  a.u., At. Data Nucl. Data Tables 49 (2) (1991) 257–314, [https://doi.org/10.1016/0092-640X\(91\)90027-2](https://doi.org/10.1016/0092-640X(91)90027-2) URL <https://www.sciencedirect.com/science/article/pii/0092640X91900272?via%3Dihub>.
- [34] S. Sakabe, Y. Izawa, Simple formula for the cross sections of resonant charge transfer between atoms and their positive ions at low impact velocity, Phys. Rev. A 45 (3) (1992) 2086–2089, <https://doi.org/10.1103/PhysRevA.45.2086> URL.
- [35] M. Hashida, S. Sakabe, Y. Izawa, Cross sections of charge transfer between a Gd atom and its singly charged positive ion in metastable states close to the ground state, Phys. Rev. A 54 (5) (1996) 4573–4576, <https://doi.org/10.1103/PhysRevA.54.4573> URL.
- [36] M. Hashida, S. Sakabe, Y. Izawa, Symmetric charge-transfer cross sections of III a rare-earth-metal elements, Phys. Rev. A 83 (3) (2011) 032704, , <https://doi.org/10.1103/PhysRevA.83.032704> URL.
- [37] D. Rapp, I.B. Ortenburger, Interchange of charge between gaseous molecules, J. Chem. Phys. 33 (4) (1960) 1230–1233, <https://doi.org/10.1063/1.1731361> URL.
- [38] S.H. Pullins, R.A. Dressier, R. Torrents, D. Gerlich, Guided-Ion beam measurements of Ar + + Ar symmetric charge-transfer cross sections at ion energies ranging from 0.2 to 300 eV, Z. Phys. Chem. 214 (36770) (2000) 1279, <https://doi.org/10.1524/zpch.2000.214.9.1279>.
- [39] M.L. Hause, B.D. Prince, R.J. Bemish, Krypton charge exchange cross sections for Hall effect thruster models, J. Appl. Phys. 113 (16) (2013) 163301, <https://doi.org/10.1063/1.4802432> URL.
- [40] S. Samaddar, S. Halder, A. Mondal, C.R. Mandal, M. Purkait, T.K. Das, Single and double electron capture in p-He and alpha-He collisions, J. Phys. B Atomic Mol. Phys. 50 (6) (2017) 065202, <https://doi.org/10.1088/1361-6455/aa5ed3> URL <http://stacks.iop.org/0953-4075/50/i=6/a=065202?key=crossref.d43dbb80fec0cb3a0e2c71861c86f787>.
- [41] E. Ghanbari-Advi, H. Ghavamian, Four-body treatment of the single-electron capture in energetic proton-helium collisions, Phys. Scr. 89 (10) (2014) 105402, <https://doi.org/10.1088/0031-8949/89/10/105402> URL <http://stacks.iop.org/1402-4896/89/i=10/a=105402?key=crossref.f4cb20c2206b4ade6932a9d9b53fc82d>.
- [42] A.L. Harris, J.L. Peacher, D.H. Madison, Theoretical fully differential cross sections for double-charge-transfer collisions, Phys. Rev. A 82 (2) (2010) 022714, <https://doi.org/10.1103/PhysRevA.82.022714> URL.
- [43] T. Baer, P.T. Murray, L. Squires, Total cross sections for symmetric charge transfer reactions of O + \_2 in selected translational and internal energy states, J. Chem. Phys. 68 (11) (1978) 4901–4906, <https://doi.org/10.1063/1.435645> URL.
- [44] W. Yang, Q. Zhou, W. Yang, Y. Dong, Z. Dong, The accuracy of collision cross sections in particle modeling on copper vacuum arcs, Cit. Phys. Plasmas 25 (063521). doi:<https://doi.org/10.1063/1.5032276>. URL <http://aip.scitation.org/toc/php/25/6>
- [45] C. Ryder, K. Minamisono, H. Asberry, B. Isherwood, P. Mantica, A. Miller, D. Rossi, R. Strum, Population distribution subsequent to charge exchange of 29.85keV Ni + on sodium vapor, Spectrochim. Acta Part B At. Spectrosc. 113 (2015) 16–21, <https://doi.org/10.1016/j.sab.2015.08.004> URL <http://linkinghub.elsevier.com/retrieve/pii/S0584854715001962>.
- [46] D.P. Dewangan, Dependence of symmetrical charge transfer cross section on ionization potential, J. Phys. B At. Mol. Phys. 6 (2) (1973) L20–L23, <https://doi.org/10.1088/0022-3700/6/2/004> URL.
- [47] D.R. Bates, H.S.W. Massey, A.L. Stewart, Inelastic collisions between atoms. I. General theoretical considerations, Proc. R. Soc. A Math. Phys. Eng. Sci. 216 (1127) (1953) 437–458, <https://doi.org/10.1088/rspa.1953.0033> URL.
- [48] N.A.T.A. Kramida, Y.Ralchenko, J. Reader, NIST Atomic Spectra Database (version 5.6), 10.18434/T4W30F, (2014) URL <http://www.nist.gov/pml/data/asd.cfm>.
- [49] D. Levin, Fast integration of rapidly oscillatory functions, J. Comput. Appl. Math. 67 (1) (1996) 95–101, [https://doi.org/10.1016/0377-0427\(94\)00118-9](https://doi.org/10.1016/0377-0427(94)00118-9).
- [50] T.E. Cocolios, R.P. de Groot, J. Billowes, M.L. Bissell, I. Budinčević, T. Day Goodacre, G.J. Farooq-Smith, V.N. Fedossev, K.T. Flanagan, S. Franchoo, R.F. Garcia Ruiz, W. Gins, H. Heylen, T. Kron, R. Li, K.M. Lynch, B.A. Marsh, G. Neyens, R.E. Rossel, S. Rothe, A.J. Smith, H.H. Stroke, K.D.A. Wendt, S.G. Wilkins, X. Yang, High-resolution laser spectroscopy with the Collinear Resonance Ionisation Spectroscopy (CRIS) experiment at CERN-ISOLDE, Nucl. Instruments Methods Phys. Res. Sect. B Beam Interact. with Mater. Atoms 376 (2016) 284–287, <https://doi.org/10.1016/j.nimb.2015.11.024>.
- [51] R.P. de Groot, M. Verlinde, V. Sonnenschein, K.T. Flanagan, I. Moore, G. Neyens, Efficient, high-resolution resonance laser ionization spectroscopy using weak transitions to long-lived excited states, Phys. Rev. A 95 (3) (2017) 032502, , <https://doi.org/10.1103/PhysRevA.95.032502> URL.
- [52] T. Kessler, H. Tomita, C. Mattolat, S. Raeder, K. Wendt, An injection-seeded high-repetition rate Ti:sapphire laser for high-resolution spectroscopy and trace analysis of rare isotopes, Laser Phys. 18 (7) (2008) 842–849, <https://doi.org/10.1134/S1054660X08070074> URL.
- [53] V. Sonnenschein, I.D. Moore, S. Raeder, M. Reponen, H. Tomita, K. Wendt, Characterization of a pulsed injection-locked Ti:sapphire laser and its application to high resolution resonance ionization spectroscopy of copper, Laser Phys. 27 (8) (2017) 085701, , <https://doi.org/10.1088/1555-6611/aa7834> URL <http://stacks.iop.org/1555-6611/27/i=8/a=085701?key=crossref.ae700ab1aa5d94924db40c8ed7febe7>.
- [54] M. Bass, P.A. Franken, A.E. Hill, C.W. Peters, G. Weinreich, Optical mixing, Phys. Rev. Lett. 8 (1) (1962) 18, <https://doi.org/10.1103/PhysRevLett.8.18> URL.
- [55] E. Mané, J. Billowes, K. Blaum, P. Campbell, B. Cheal, P. Delahaye, K.T. Flanagan, D.H. Forest, H. Franberg, C. Geppert, T. Giles, A. Jokinen, M. Kowalska, R. Neugart, G. Neyens, W. Nörterhäuser, I. Podadera, G. Tungate, P. Vingerhoets, D.T. Yordanov, An ion cooler-buncher for high-sensitivity collinear laser spectroscopy at ISOLDE, Eur. Phys. J. A 42 (3) (2009) 503–507, <https://doi.org/10.1140/epja/i2009-10-828-0>.
- [56] R.P. de Groot, I. Budinčević, J. Billowes, M.L. Bissell, T.E. Cocolios, G.J. Farooq-Smith, V.N. Fedossev, K.T. Flanagan, S. Franchoo, R.F. Garcia Ruiz, H. Heylen, R. Li, K.M. Lynch, B.A. Marsh, G. Neyens, R.E. Rossel, S. Rothe, H.H. Stroke, K.D.A. Wendt, S.G. Wilkins, X. Yang, Use of a continuous wave laser and pockels cell for sensitive high-resolution collinear resonance ionization spectroscopy, Phys. Rev. Lett. 115 (13) (2015) 132501, <https://doi.org/10.1103/PhysRevLett.115.132501> URL.
- [57] A. Voss, M.R. Pearson, J. Billowes, F. Buchinger, B. Cheal, J.E. Crawford, A.A. Kwiatkowski, C.D.P. Levy, O. Shelbaya, First use of high-frequency intensity modulation of narrow-linewidth laser light and its application in determination of 206,205,204Fr ground-state properties, Phys. Rev. Lett. 111 (12) (2013) 122501, , <https://doi.org/10.1103/PhysRevLett.111.122501> URL.
- [58] C. Levy, T. Cocolios, J. Behr, K. Jayamanna, K. Minamisono, M. Pearson, Feasibility study of in-beam polarization of fluorine, Nucl. Instruments Methods Phys. Res. Sect. A Accel. Spectrometers, Detect. Assoc. Equip. 580 (3) (2007) 1571–1577, <https://doi.org/10.1016/j.nima.2007.07.013>.
- [59] D. Hanstorp, A secondary emission detector capable photoelectric effect induced by

- pulsed lasers, *Meas. Sci. Technol.* 3 (5) (1992) 523–527, <https://doi.org/10.1088/0957-0233/3/5/013> URL <http://stacks.iop.org/0957-0233/3/i=5/a=013>.
- [60] S. Rothe, J. Sundberg, J. Welander, K. Chrysalidis, T.D. Goodacre, V. Fedossev, S. Fiotakis, O. Forstner, R. Heinke, K. Johnston, T. Kron, U. Köster, Y. Liu, B. Marsh, A. Ringvall-Moberg, R.E. Rossel, C. Seiffert, D. Studer, K. Wendt, D. Hanstorp, Laser photodetachment of radioactive  $^{128}\text{I}$  – laser photodetachment of radioactive, *J. Phys. G Nucl. Part. Phys.* 44 (10) (2017) 104003, <https://doi.org/10.1088/1361-6471/aa80aa> URL <http://stacks.iop.org/0954-3899/44/i=10/a=104003?key=crossref.853522bbb0fcabbb7110d8ae82ed31a8>.
- [61] O.B. Firsov, A qualitative interpretation of the mean electron excitation energy in atomic collisions, *J. Exptl. Theor. Phys.* 36 (36) (1959) 1517–1523.
- [62] A. Kumar, R. Kanungo, A. Calci, P. Navatil, A. Sanetullaev, M. Alcorta, V. Bildstein, G. Christian, B. Davids, J. Dohet-Eraly, J. Fallis, A.T. Gallant, G. Hackman, B. Hadinia, G. Hupin, S. Ishimoto, R. Krucken, A.T. Laffoley, J. Lighthall, D. Miller, S. Quaglioni, J.S. Randhawa, E.T. Rand, A. Rojas, R. Roth, A. Shotter, J. Tanaka, I. Tanihata, C. Unsworth, Nuclear force imprints revealed on the elastic scattering of protons with C 10, *Phys. Rev. Lett.* 118 (26) (2017) 262502, , <https://doi.org/10.1103/PhysRevLett.118.262502> URL .
- [63] B.J. Wood, A.N. Halliday, The lead isotopic age of the Earth can be explained by core formation alone, *Nature* 465 (7299) (2010) 767–770, <https://doi.org/10.1038/nature09072> URL <http://www.nature.com/articles/nature09072>.
- [64] Z. Wang, H. Becker, Ratios of S, Se and Te in the silicate Earth require a volatile-rich late veneer, *Nature* 499 (7458) (2013) 328–331, <https://doi.org/10.1038/nature12285> URL <http://www.nature.com/articles/nature12285>.
- [65] T. Naeraa, A. Scherstén, M.T. Rosing, A.I.S. Kemp, J.E. Hoffmann, T.F. Kokfelt, M.J. Whitehouse, Hafnium isotope evidence for a transition in the dynamics of continental growth 3.2 Gyr ago, *Nature* 485 (7400) (2012) 627–630, <https://doi.org/10.1038/nature11140> URL <http://www.nature.com/articles/nature11140>.
- [66] R.F. Garcia Ruiz, INTC-I-189 Laser Spectroscopy Studies of Light Nuclei, URL, May 2017. <https://cds.cern.ch/record/2266804?ln=bg>.
- [67] T. Stöhlker, T. Ludziejewski, H. Reich, F. Bosch, R.W. Dunford, J. Eichler, B. Franzke, C. Kozhuharov, G. Menzel, P.H. Mokler, F. Nolden, P. Rymuza, Z. Stachura, M. Steck, P. Swiat, A. Warczak, T. Winkler, Charge-exchange cross sections and beam lifetimes for stored and decelerated bare uranium ions, *Phys. Rev. A* 58 (3) (1998) 2043–2050, <https://doi.org/10.1103/PhysRevA.58.2043> URL .
- [68] I. Dillmann, M. Hannawald, U. Köster, V.N. Fedoseyev, A. Wöhrl, B. Pfeiffer, D. Fedorov, J. Shergur, L. Weissman, W.B. Walters, K.L. Kratz, Selective laser ionization of  $N = > 82$  indium isotopes: the new r-process nuclide  $^{135}\text{In}$ , *Eur. Phys. J. A* 13 (3) (2002) 281–284, <https://doi.org/10.1007/s10050-002-8756-7>.
- [69] C. Schulz, E. Arnold, W. Borchers, W. Neu, R. Neugart, M. Neuroth, E.W. Otten, M. Scherf, K. Wendt, P. Lievens, Y.A. Kudryavtsev, V.S. Letokhov, V.I. Mishin, V.V. Petrunin, Resonance ionization spectroscopy on a fast atomic ytterbium beam, *J. Phys. B Atomic Mol. Phys.* 24 (22) (1991) 4831–4844, <https://doi.org/10.1088/0953-4075/24/22/020> URL <http://stacks.iop.org/0953-4075/24/i=22/a=020?key=crossref.2c87f8c494d942077faa53dbed7374f5>.
- [70] J.-L. Picqué, J.-L. Vialle, Atomic-beam deflection and broadening by recoils due to photon absorption or emission, *Opt. Commun.* 5 (5) (1972) 402–406, [https://doi.org/10.1016/0030-4018\(72\)90043-0](https://doi.org/10.1016/0030-4018(72)90043-0) URL <https://www.sciencedirect.com/science/article/pii/0030401872900430>.
- [71] N. Bendali, H.T. Duong, P. Juncar, J.M.S. Jalm, J.L. Vialle, Na + -Na charge exchange processes studied by collinear laser spectroscopy, *J. Phys. B At. Mol. Phys.* 19 (2) (1986) 233–238, <https://doi.org/10.1088/0022-3700/19/2/012> URL <http://stacks.iop.org/0022-3700/19/i=2/a=012?key=crossref.0316417702b9b9d983b24575ea475f88>.
- [72] J. Olivero, R. Longbothum, Empirical fits to the Voigt line width: a brief review, *J. Quant. Spectrosc. Radiat. Transf.* 17 (2) (1977) 233–236, [https://doi.org/10.1016/0022-4073\(77\)90161-3](https://doi.org/10.1016/0022-4073(77)90161-3) URL <https://www.sciencedirect.com/science/article/pii/0022407377901613>.